NEUROSCIENCE

Distinct septo-hippocampal cholinergic projections separately mediate stress-induced emotional and cognitive deficits

Jian-Lin Wu†, Zi-Ming Li†, Hao Chen, Wen-Jun Chen, Neng-Yuan Hu, Shi-Yang Jin, Xiao-Wen Li, Yi-Hua Chen, Jian-Ming Yang, Tian-Ming Gao*

Patients suffering from chronic stress develop numerous symptoms, including emotional and cognitive deficits. The precise circuit mechanisms underlying different symptoms remain poorly understood. We identified two distinct basal forebrain cholinergic subpopulations in mice projecting to the dorsal hippocampus (dHPC) or ventral hippocampus (vHPC), which exhibited distinct input organizations, electrophysiological characteristics, transcriptomics, and responses to positive and negative valences of stimuli and were critical for cognitive and emotional modulation, respectively. Moreover, chronic stress induced elevated anxiety levels and cognitive deficits in mice, accompanied by enhanced vHPC but suppressed dHPC cholinergic projections. Chemogenetic activation of dHPC or inhibition of vHPC cholinergic projections alleviated stress-induced aberrant behaviors. Furthermore, we identified that the acetylcholinesterase inhibitor donepezil combined with blockade of muscarinic receptor 1–type muscarinic acetylcholine receptors in the vHPC rescued both stress-induced phenotypes. These data illuminated distinct septo-hippocampal cholinergic circuits mediated specific symptoms independently under stress, which may provide promising strategies for circuit-based treating of stress-related psychiatric disorders.

INTRODUCTION

Maladaptive responses to prolonged stress are associated with the onset and exacerbation of neuropsychiatric disorders, and chronic exposure to stress can notably alter brain function, leading to emotional symptoms such as anxiety and depression (*1*, *2*). In addition to emotional symptoms, patients commonly experience other symptoms, including cognitive deficits (*3*, *4*). The variable set of symptoms related to stress poses a challenge to achieving successful and sustained treatment. The diversity of behavioral symptoms suggests that discrete phenotypes under stress may be mediated by distinct circuit elements. However, it remains unclear how different areas are interconnected or how these circuits contribute to specific behavioral domains. Therefore, the identification of neural circuit mechanisms responsible for distinct stress-related symptoms may ultimately facilitate the development of innovative therapeutic interventions.

The hippocampal region is implicated in both cognitive and affective modulation. The medial septum and ventral diagonal band of Broca (MS/vDB) located in the basal forebrain are anatomically and functionally associated with the hippocampal formation (*5*, *6*). Previous studies have established a notable correlation between the MS/vDB and cognitive function (*5*, *7*–*9*). In addition, it has been suggested that the MS/vDB may also affect affective behaviors (*10*–*12*). Multiple lines of evidence suggest the involvement of the MS/vDB in the stress response. Anatomical evidence indicates that MS/vDB neurons receive inputs from hypothalamic and brain stem regions, including the lateral hypothalamus (LH) and periaqueductal gray, which are involved in stress-related behaviors (*13*–*15*). Mice exposed to stress exhibited heightened activity in the MS/vDB (*16*, *17*). Exposure to stressors can trigger an immediate response from the autonomic nervous system (*18*). Studies have demonstrated a correlation between the activity of MS neurons and elevated blood pressure (*19*–*21*). Furthermore, in vivo recordings have demonstrated that the activation of MS neurons is induced by noxious peripheral stimulation (*22*). A more recent study indicated that MS glutamatergic neurons mediate the influence of sensory cues on aversive emotions (*11*). Moreover, emerging evidence suggests that corticotropin-releasing factor (CRF), a neuropeptide associated with stress, modulates stress-induced cognitive impairments through its receptors in the MS (*23*–*25*). Together, these investigations propose that the MS/vDB plays a pivotal role in the stress response. However, the mechanisms underlying adaptive changes in MS/vDB neurons in response to chronic stress remain unknown, and it is unclear if precise circuit-specific organization and function of the MS/vDB contribute to stress-related psychiatric disorders.

Cholinergic neurons [choline acetyltransferase (ChAT) neurons] in the MS/vDB provide the major cholinergic innervation to the hippocampus through the fimbria-fornix pathway (*26*). Although the hippocampus is widely recognized as a crucial brain region in modulating the stress response (*27*–*29*), there is a scarcity of studies that have directly examined the function of the septo-hippocampal cholinergic circuit under stress. Furthermore, while multiple lines of evidence demonstrate the necessity of MS/vDB ChAT neurons in cognitive processes (*5*, *30*–*32*), other studies suggest that these neurons bidirectionally modulate emotional behaviors (*12*, *33*). Because of the notable cellular heterogeneity of MS/vDB ChAT neurons (*34*, *35*), it remains unclear if distinct cholinergic subpopulations within the MS/vDB contribute separately to stress-induced emotional and cognitive disorders.

Acetylcholinesterase inhibitors (AChEIs), which enhance cholinergic function by increasing the level of acetylcholine (ACh), are widely used for treating cognitive deficits in patients with Alzheimer's disease or Parkinson's disease (*36*). A clinical study revealed that the administration of AChEIs to normal volunteers resulted in notable increases in plasma cortisol levels (*37*). In addition, several

State Key Laboratory of Organ Failure Research, Key Laboratory of Mental Health of the Ministry of Education, Guangdong-Hong Kong-Macao Greater Bay Area Center for Brain Science and Brain-Inspired Intelligence, Guangdong-Hong Kong Joint Laboratory for Psychiatric Disorders, Guangdong Provincial Key Laboratory of Psychiatric Disorders, Guangdong Basic Research Center of Excellence for Integrated Traditional and Western Medicine for Qingzhi Diseases, Department of Neurobiology, School of Basic Medical Sciences, Southern Medical University, Guangzhou, China.
*Corresponding author. Email: tgao@smu.edu.cn
†These authors contributed equally to this work.

studies have indicated that acute AChEI administration in participants enhanced their anxiety state (*38*–*41*). Animal studies have also demonstrated that AChEIs, such as donepezil, can lead to an elevation in anxiety levels (*42*, *43*). However, the precise target region of AChEIs in anxiogenic-like effects remains to be elucidated.

In the present study, we identified that ChAT neurons projecting to the dorsal hippocampus (dHPC) or ventral hippocampus (vHPC) in the MS/vDB represent two distinct subpopulations, exhibiting different anatomical structures, electrophysiological characteristics, responses to aversive and appetitive stimuli, and functional properties. These two distinct subpopulations display contrasting electrophysiological and transcriptional adaptations in response to chronic restraint stress. Furthermore, we report that distinct cholinergic circuits are responsible for cognitive deficits and heightened anxiety states in stress mice. Furthermore, we have identified that the combination of donepezil and application of a muscarinic receptor 1 (M1) antagonist in the vHPC can effectively rescue both stress-induced phenotypes.

RESULTS

The MS/vDB ChAT neurons transmit negative valence signals

We used a Cre-dependent GCaMP6m calcium indicator expressed virally in ChAT-ires-Cre mice and monitored changes in the fluorescence signal using an optic fiber above the MS/vDB (Fig. 1A). The histological analysis showed that over 90% of GCaMP6m-expressing cells were located and colocalized with ChAT-positive cells in the MS/vDB of mice used for calcium imaging experiments

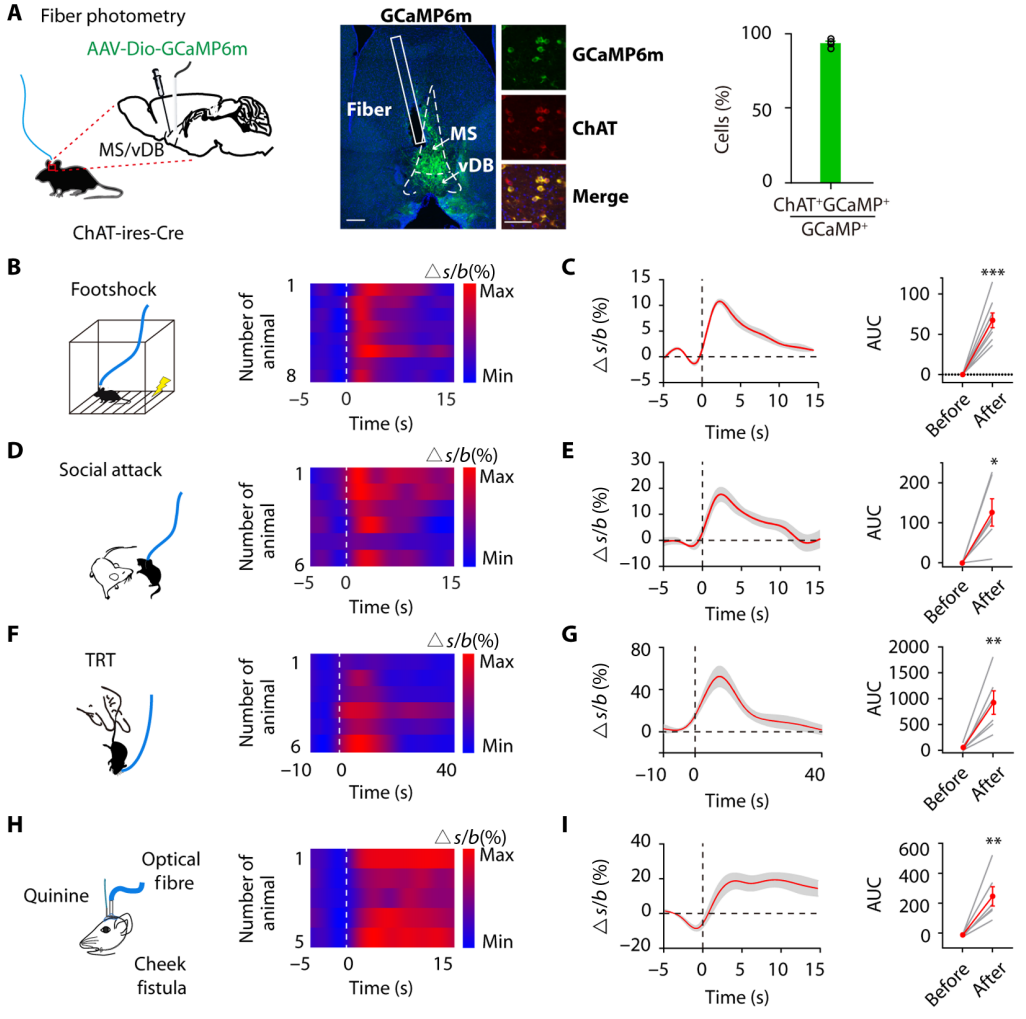

Fig. 1. Aversive stimuli elicit MS/vDB ChAT neuronal activity. (**A**) (Left) Fiber photometry setup. (Middle) GCaMP6m expression and optical fiber tract in the MS/vDB. Scale bar, 200 μm. (Further right) Overlap between GCaMP6m-expressing cells (green) and anti–ChAT-positive cells (red). Scale bar, 50 μm. (Right) Percentage of GCaMP6m+ neurons coexpressing ChAT. (**B**) (Left) Schematic for footshock. (Right) Heatmap of Ca^{2+} transients across animals aligned to the start of footshock. (**C**) (Left) Plot of Ca^{2+} transients across animals aligned to the start of footshock. (Right) Change in calcium signals. $n = 8$ mice, AUC, area under the curve. (**D**) (Left) Schematic for social attack. (Right) Heatmap plot of Ca^{2+} transients across animals aligned to the start of attack. (**E**) (Left) Plot of Ca^{2+} transients across animals aligned to the start of attack. (Right) Change in calcium signals. $n = 6$ mice. (**F**) (Left) Schematic for TRT application. (Right) Heatmap plot of Ca^{2+} transients across animals aligned to the start of the TRT. (**G**) (Left) Plot of Ca^{2+} transients across animals aligned to the start of the TRT. (Right) Change in calcium signals. $n = 6$ mice. (**H**) (Left) Schematic of intraoral quinine infusion. (Right) Heatmap of Ca^{2+} transients across animals aligned to the start of quinine infusion. (**I**) (Left) Plot of Ca^{2+} transients across animals aligned to the start of quinine infusion. (Right) Change in calcium signals. $n = 6$ mice. Paired *t* test. $^{*}P < 0.05$; $^{**}P < 0.01$; $^{***}P < 0.001$. Data are presented as the means ± SEM.

(Fig. 1A and fig. S1, A and B). The expression of GCaMP6m was observed in 31% of ChAT neurons in the MS/vDB (fig. S1C).

We initially investigated alterations in GCaMP6m fluorescence intensity under aversive stimuli. During a footshock test, in which mice were randomly subjected to four electric shocks (0.75 mA, 2 s), we observed a rapid increase in GCaMP6m intensity following the footshock (Fig. 1, B and C). Similar outcomes were observed in the context of social aggression (Fig. 1, D and E). During the tail restraint test (TRT), GCaMP6m intensity increased when mice were manually chased and lifted, indicating a heightened neuronal response to physical stimulation (Fig. 1, F and G). Then, intraoral cheek fistulae were implanted into the oral cavity of mice for delivery of a quinine solution (5 mM, 10 μl in 0.5 s) (Fig. 1H). Notably, the administration of quinine resulted in a notable enhancement of GCaMP6m fluorescence intensity (Fig. 1, H and I). However, the fluctuations in GCaMP6m fluorescence intensity showed no obvious correlation with the velocity of mice (fig. S1D). Furthermore, mice with MS/vDB ChAT neurons expressing enhanced green fluorescent protein (EGFP) exhibited negligible changes in fluorescence intensity during the TRT or footshock stimuli (fig. S1, E to G), indicating that the observed alterations in $\Delta F/F$ were not attributable to movement artifacts.

We then investigated the responsiveness of MS/vDB ChAT neurons to reward stimuli. Water-deprived mice received sucrose by licking a nozzle. Contrary to previous findings indicating that reward enhances ChAT neuron activity in the horizontal limb of the diagonal band of Broca (hDB) (*44*–*46*), we observed a notable decrease in GCaMP6m intensity following sucrose licking (fig. S1). To mitigate the potential impact of signal attenuation over time, we administered a 5% w/v sucrose solution (10 ml in 0.5 s) into the oral cavity of water-deprived mice. The delivery of sucrose consistently suppressed GCaMP6m signals in MS/vDB- ChAT^{GCaMP6m} mice (fig. S1J). Relevant findings were also observed in the context of food intake (fig. S1L). Notably, mice with MS/vDB ChAT neurons expressing EGFP exhibited no obvious changes in fluorescence intensity during reward stimuli, excluding the possible hemodynamic contamination of photometry signals (fig. S1, I and K). These observations suggest that MS/vDB ChAT neurons exhibit responsiveness to a broad spectrum of aversive stimuli and can be suppressed by appetitive reward.

We then used optogenetics to investigate the impact of activating MS/vDB ChAT neurons in a real-time place avoidance (RTPA) assay. We administered a Cre-dependent adeno-associated virus (AAV) channelrhodopsin-2 (ChR2) fused to mCherry (AAV-Dio-ChR2-mCherry) or a control virus carrying only mCherry into the MS/vDB of ChAT-ires-Cre mice (Fig. 2A). We confirmed the activation of MS/vDB ChAT neurons by blue light stimulation (Fig. 2B). ChR2-expressing animals displayed a reduced preference for the stimulation chamber compared to the control chamber (Fig. 2C). Moreover,

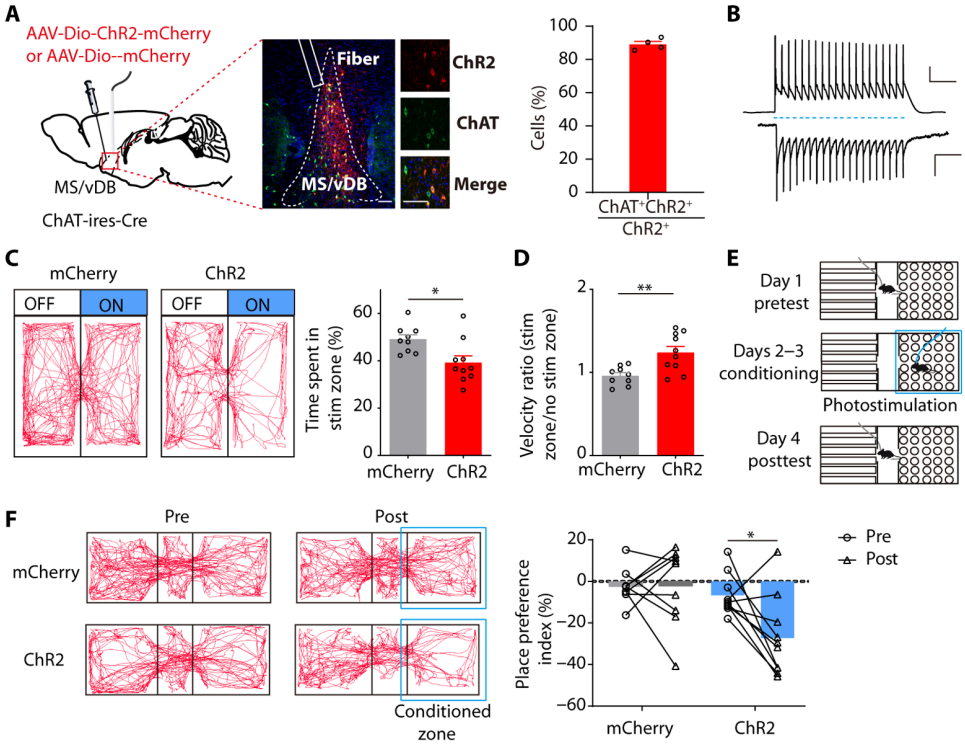

Fig. 2. Activation of MS/vDB ChAT neurons induces place avoidance. (**A**) (Left) Schematic of viral injection and optical fiber implantation site. (Middle) ChR2 expression in ChAT neurons and the optical fiber tract above the MS/vDB. Scale bar, 100 μm. (Further right) Overlap between ChR2-expressing cells (red) and anti–ChAT-positive cells (green). Scale bar, 20 μm. (Right) Percentage of GCaMP6m+ neurons coexpressing ChAT ($n = 4$ mice). (**B**) Response of a ChR2 cell to a train of light pulses (20 Hz, 10-ms pulse width; blue dashed line) for 1 s in current clamp (top; scale bar, 20 mV, 200 ms) and voltage clamp (bottom; scale bar, 200 pA, 200 ms) mode. (**C**) (Left) Representative locomotor traces of mCherry and ChR2 mice in an RTPA. (Right) Time spent in the stimuli zone of mice. mCherry, $n = 9$; ChR2, $n = 10$; unpaired t test. (**D**) Velocity ratio of mice. mCherry, $n = 9$; ChR2, $n = 10$; unpaired t test. (**E**) Schematic for the conditioned place preference experiment. (**F**) (Left) Movement tracking traces for the mCherry mouse and ChR2 mouse in pretest and posttest. (Right) Individual place preference indices (%) of mice before and after conditioning. mCherry, $n = 9$; ChR2, $n = 9$; two-way ANOVA with Holm-Sidak post hoc analysis. $^*P < 0.05$; $^{**}P < 0.01$. Data are presented as the means ± SEM.

we observed that ChR2-expressing animals exhibited increased locomotor activity on the stimulated side compared to control (Fig. 2D). Furthermore, we used a Pavlovian conditioned place aversion assay to directly assess the enduring learned associations resulting from the activation of MS/vDB ChAT neurons (Fig. 2E). Following 2 days of photostimulation conditioning, ChR2-expressing animals spent notably less time in the context previously paired with photostimulation (Fig. 2F). The findings collectively support the proposition that the activation of MS/vDB ChAT neurons is indicative of negative valence.

MS/vDB ChAT neurons process and regulate the anxiety state

The aforementioned findings suggest the enhanced activity of MS/vDB ChAT neurons eliciting defensive reactions in animals. To investigate the involvement of MS/vDB ChAT neurons in spontaneous avoidance, we recorded their activity in the elevated plus maze (EPM). The activity of MS/vDB ChAT neurons increased before mice entered the anxiogenic open-arm compartment and remained high while mice explored the open arms (Fig. 3, A to C). The observed increase in activity cannot be attributed to differences in mouse velocity between compartments as the open-arm and closed-arm velocities were comparable across all animals (fig. S2A). Furthermore, exploration of the quadrant containing the novel object did not result in increased MS/vDB ChAT neuronal activity (fig. S2, B to D), indicating a bias of these neurons toward representing anxiogenic features rather than spatial salience changes.

We subsequently investigated if the open arm–induced activity of MS/vDB ChAT neurons was essential for maintaining avoidance behavior in the EPM. We injected control virus or one that expressed enhanced natronomonas pharaonis halorhodopsin (eNpHR, used for optogenetic inhibition) into the MS/vDB of ChAT-ires-Cre mice and implanted fiber optics (Fig. 3D). Yellow light induced the inhibition of MS/vDB eNpHR-expressing neuronal activity (Fig. 3E). The

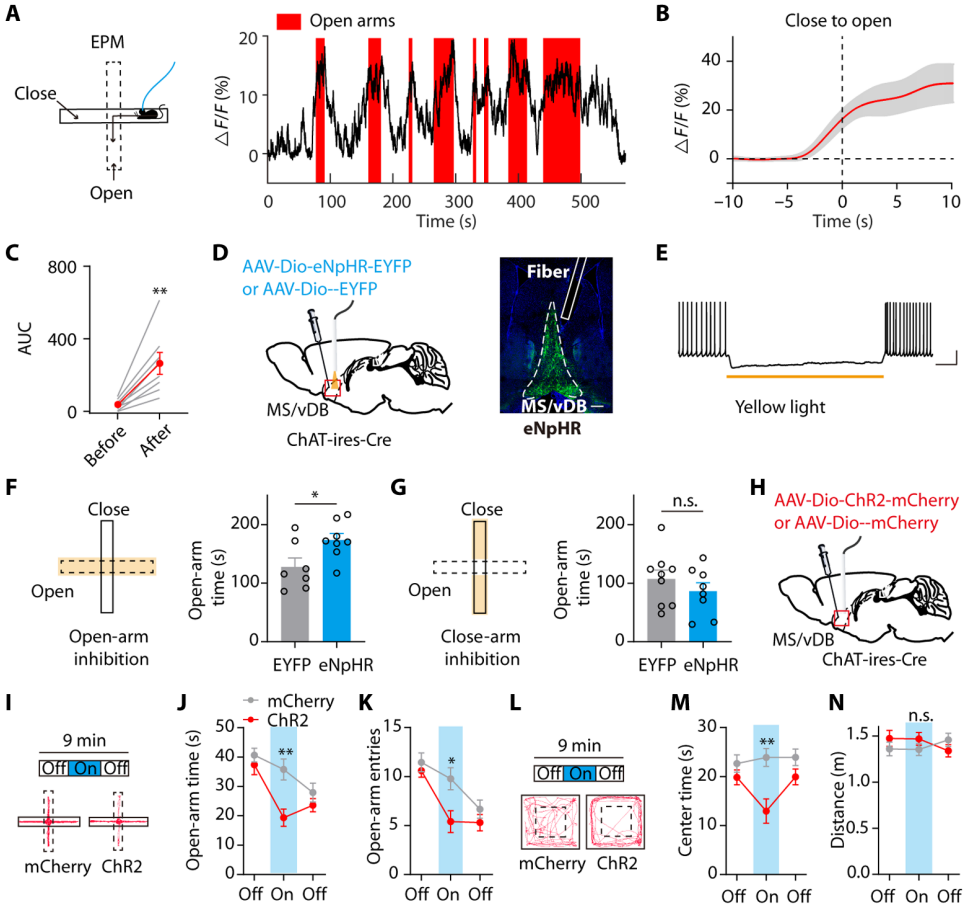

Fig. 3. The MS/vDB ChAT neurons process and modulate anxiety-like behaviors. (**A**) (Left) Ca^{2+} recording during the EPM test. (Right) Example of MS/vDB ChAT neuronal activity within the EPM. (**B**) Plot of Ca^{2+} transients aligned to the start of open-arm entry. $n = 8$. (**D**) Change in Ca^{2+} signals. $n = 8$. (**D**) (Left) Virus injection and fiber implantation for optogenetic inhibition of MS/vDB ChAT neurons. (Right) Representative image illustrating eNpHR-expressing cells and the fiber tract in the MS/vDB. Scale bar, 200 μm. (**E**) Response of an eNpHR cell to yellow light illumination under 30 pA of current injection. (**F** and **G**) The laser was triggered on when mice entered the open or closed arms only. Open-arm silencing increased the time spent exploring the open arms [(F) EYFP, $n = 7$; eNpHR, $n = 8$]. Silencing in the closed arms had no effect [(G) EYFP, $n = 9$; eNpHR, $n = 8$]. (**H**) Schematic of viral expression and implantation site. (**I**) Representative tracks during the illumination epoch within the EPM for ChR2 mouse and mCherry mouse. (**J** and **K**) Light activation of MS/vDB ChAT neurons resulted in a decrease in the duration mice spent exploring the open arms [(J) mCherry, $n = 9$; ChR2, $n = 10$] and the open-arm entries (K). (**L**) Representative tracks during the illumination epoch within the OFT for ChR2 mouse and mCherry mouse. (**M**) Time spent in exploring the center in the OFT. (**N**) Distance traveled in the OFT. Paired *t* test for (C); unpaired *t* test for (F) and (G); two-way, repeated-measures ANOVA with Bonferroni's post hoc analysis for (J), (K), (M), and (N). $^*P < 0.05$; $^{**}P < 0.01$. Data are presented as the means ± SEM. n.s., not significant.

ChAT neuronal activity in the MS/vDB was selectively inhibited only when mice entered the center and open arms of the EPM; mice expressing eNpHR spent a notably greater amount of time exploring the open arms of the EPM (Fig. 3F). The closed-arm silencing did not affect the open-arm avoidance behavior, unlike the open-arm silencing in the EPM (Fig. 3G). Moreover, this was not attributable to the appetitive effects of MS/vDB ChAT neurons inhibition in the open arms as both groups exhibited similar preference for the side with light illumination in a real-time place preference assay (fig. S2E).

In addition, we investigated if enhanced ChAT neuronal activity in the MS/vDB would affect anxiety levels during the EPM and another open field test (OFT). AAV-Dio-ChR2-mCherry or a control virus carrying mCherry was injected into the MS/vDB of ChAT-ires-Cre mice (Fig. 3H and fig. S15A). In the EPM test, the animal tracks representative of the light-on epoch from both ChR2 and mCherry groups are presented (Fig. 3I). Mice in the ChR2 group displayed a reduction in open-arm exploration and entering into the open arms (Fig. 3, J and K), indicating an elevated anxiety state during the On epoch. Similar to the findings in the EPM, ChR2 mice exhibited reduced center exploration compared to control mice during On epoch illumination in the OFT (Fig. 3, L and M). Reassessing locomotor activity across epochs failed to reveal any alterations in distance traveled during the On epoch (Fig. 3N). These findings suggest that ChAT neuronal activity in the MS/vDB region may serve as a signal and regulator of anxiety states.

MS/vDB ChAT neurons exhibit distinct subpopulations projecting to the dHPC and vHPC regions

Consistent with previous findings (*47*), our results indicate that MS/vDB ChAT neurons exhibit dense innervation in both the dHPC and vHPC regions (fig. S3, A to C). Do individual MS/vDB ChAT neurons send collateralized axons to target both the dHPC and vHPC, or do dHPC-projecting and vHPC-projecting MS/vDB ChAT neurons represent distinct subpopulations (Fig. 4A)? To ascertain if the MS/vDB ChAT neurons projecting to the dHPC and vHPC are identical or distinct entities, Cre-inducible, retrogradely trafficked viral vectors were injected into the dorsal CA1 (dCA1) (AAV_{retro}-Dio-EYFP) and ventral CA1 (vCA1) (AAV_{retro}-Dio-mCherry), respectively (Fig. 4B). Most CA1-projecting ChAT neurons were located in the MS/vDB (fig. S3D). We observed distinct neuronal populations projecting to the dCA1 and vCA1 regions with minimal overlap (Fig. 4C), and they were distributed in an anterior-posterior axis with a salt-and-pepper pattern (Fig. 4D). We also injected cholera toxin subunit B (CTB) conjugated to Alexa Fluor 488 or 555 into the dCA1 or vCA1 and quantified neurons that were double labeled for ChAT and CTB (fig. S3E). Once again, we identified two distinct populations of neurons projecting to either the dCA1 or vCA1 regions (fig. S3, F and G). Moreover, ex vivo electrophysiological recordings revealed that ChAT neurons projecting to vCA1 had lower intrinsic excitability than those projecting to dCA1 (Fig. 4, E and F). Consistently, the threshold and after-hyperpolarization amplitude of the ChAT neurons projecting to vCA1 were greater than those of ChAT neurons projecting to dCA1 (fig. S3, H to O).

We subsequently examined the output domains of these distinct subpopulations of ChAT neurons (Fig. 4G). The analysis of the axonal fibers within the hippocampus revealed that dCA1-projecting MS/vDB ChAT neurons project to dCA1, dorsal dentate gyrus (dDG), and dCA3 with a similar extent, whereas vCA1-projecting MS/vDB ChAT neurons mainly innervate vCA1 and vCA3 (Fig. 4H and fig. S4). Then, we used cell type–specific and projection-specific transsynaptic tracing to examine the input organization of dCA1-projecting and vCA1-projecting MS/vDB ChAT neurons (Fig. 4I). Quantification of mCherry-labeled neurons across the entire brain revealed notable differences in the input regions to these two neuronal populations. Specifically, dCA1-projecting MS/vDB ChAT neurons exhibit a relatively higher degree of input from the subiculum and lateral entorhinal cortex (LEnT) regions, whereas vCA1-projecting MS/vDB ChAT neurons demonstrate a notably greater level of input from areas such as the hypothalamic arcuate nucleus (ARC) and dorsal raphe nucleus (DRN) (Fig. 4, J and K). Moreover, we observed that most DRN neurons projecting to these two neuronal populations are nonserotonergic (fig. S5A), whereas the vast majority of ventral tegmental area neurons innervating these two neuronal populations are dopaminergic (fig. S5B). Furthermore, a previous study identified $D28K^+$ ChAT neurons in the MS that target vCA1 pyramidal cells (*48*). Consistently, we observed ~30% of vCA1-projecting MS/vDB ChAT neurons expressing D28K (fig. S6). As the targets of dCA1 or vCA1-projecting MS/vDB ChAT neurons in the hippocampus can be classified into dorsal and ventral groups, therefore, MS/vDB ChAT neurons projecting to the dCA1 will be referred to as $ChAT^{MS/vDB\text{-}dHPC}$ neurons and MS/vDB ChAT neurons projecting to vCA1 as $ChAT^{MS/vDB\text{-}vHPC}$ neurons hereafter.

MS/vDB cholinergic input to the vHPC and the dHPC regions separately modulates anxiety-like behaviors and spatial learning and memory

We next investigated the activity of cholinergic fibers from the MS/vDB to vHPC (Fig. 5A). Histological analysis revealed that more than 90% of GCaMP6s-expressing cells colocalized with ChAT-positive cells in the MS/vDB (Fig. 5B). An optical fiber was implanted above the vHPC region (Fig. 5C). Recording data from the EPM indicate that there is a rapid activation of MS/vDB-vHPC ChAT fibers prior to mice entering the open arms, and these fibers exhibit higher activity during mice exploration of the open arms (Fig. 5, D and E). Moreover, this projection is also activated by aversive stimuli (fig. S7, A and B) and suppressed by sucrose reward (fig. S7C). Hence, we proceeded to investigate if cholinergic projection activity from the MS/vDB-vHPC contributes to anxiety-related behaviors (Fig. 5F and fig. S15B). The results showed that selective inhibition of cholinergic projections from the MS/vDB-vHPC during open-arm, but not closed-arm exploration, effectively attenuated the open-arm avoidance behavior in the EPM (Fig. 5, G and H).

Subsequently, we evaluated if elevation of MS/vDB-vHPC cholinergic projection activity through optogenetics could potentiate the anxiety state (figs. S7D and S15E). Optogenetic stimulation resulted in notably higher levels of corticosterone (CORT) in mice injected with ChR2 than mCherry mice (fig. S7E). In the RTPA test, ChR2-expressing animals displayed a reduced preference for the stimulation chamber (fig. S7F). Furthermore, the activation of MS/vDB-vHPC cholinergic projection resulted in a decrease in the time spent and entries made into the open arms (fig. S7, G to I). In the OFT, light activation also decreased the time spent in the center while having no effect on mouse locomotion (fig. S7, J to L).

To further determine if ACh release from the MS/vDB-vHPC cholinergic pathway contributes to the induction of the anxiety-like behaviors, we applied cholinergic receptor antagonists, including a nicotinic receptor antagonist, 0.2 μl of mecamylamine (0.5 μg) together with a muscarinic receptor antagonist, atropine (1.0 μg), into the vHPC of mice 1 hour before the behavioral tests. This treatment effectively blocked the behavioral phenotypes induced by the chemogenetic activation of MS/

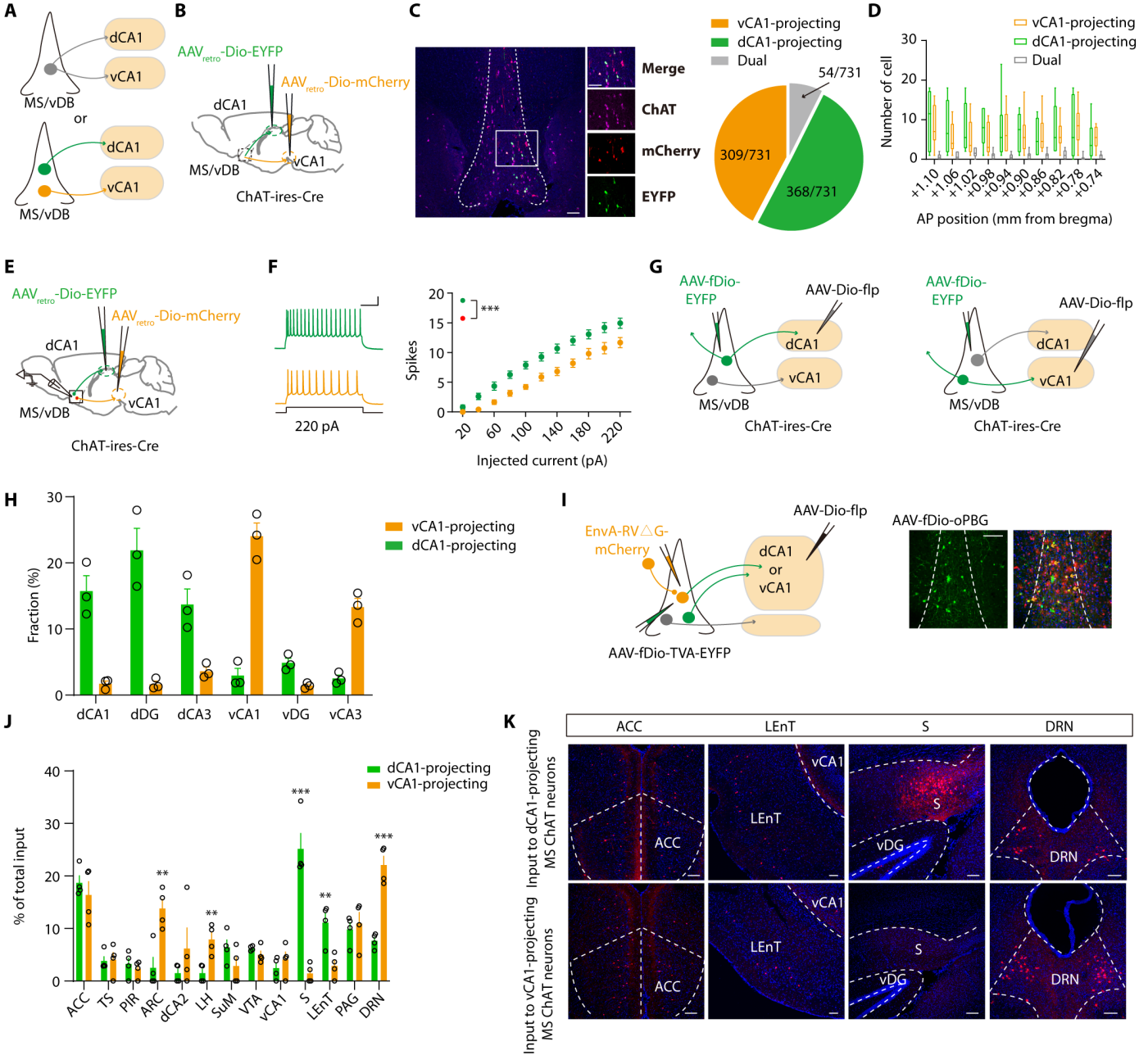

Fig. 4. Distinct subpopulations of MS/vDB ChAT neurons project to the dCA1 and vCA1. (**A**) Two possible projection patterns. (**B**) Dual retrovirus strategy used for labeling dCA1-projecting or vCA1-projecting MS/vDB ChAT neurons. (**C**) (Left) EYFP and mCherry expression in MS/vDB ChAT neurons (purple). Scale bar, 100 μm. (Right) Proportion of cells classified as projecting to the dCA1, vCA1, or both (731 cells from four mice). (**D**) Number of dCA1-projecting and vCA1-projecting ChAT neurons throughout the anterior-posterior (AP) extent of the MS/vDB. (**E**) Ex vivo recording of dCA1-projecting or vCA1-projecting MS/vDB ChAT neurons. (**F**) Representative traces (left) and injected current-evoked firing relationship (right) of dCA1-projecting or vCA1-projecting MS/vDB ChAT neurons. Scale bar, 100 ms, 20 mV. Two-way, repeated-measures ANOVA with Bonferroni's post hoc analysis. (**G**) Viral strategy used for tracing the output of $ChAT^{MS/vDB\text{-}dCA1}$ or $ChAT^{MS/vDB\text{-}vCA1}$ neurons. (**H**) Fiber quantitation of dCA1-projecting or vCA1-projecting MS/vDB ChAT neurons. (**I**) (Left) Strategy to map monosynaptic inputs to either $ChAT^{MS/vDB\text{-}dCA1}$ or $ChAT^{MS/vDB\text{-}vCA1}$ neurons. (Right) Starter cell localization of AAV-fDio-EYFP-TVA, AAV-fDio-oPBG, and EnvA-RV△G-mCherry (yellow arrows). Scale bar, 100 μm. (**J**) Whole-brain quantitation of inputs to $ChAT^{MS/vDB\text{-}dCA1}$ and $ChAT^{MS/vDB\text{-}vCA1}$ neurons. Percentage of total cells in a given brain area relative to the total number of brain-wide inputs. $n = 4$ for each condition, unpaired t test. (**K**) Representative images of inputs in select brain areas. ACC, anterior cingulate cortex. Scale bars, 100 μm. $^{**}P < 0.01$; $^{***}P < 0.001$. Data are presented as the means ± SEM.

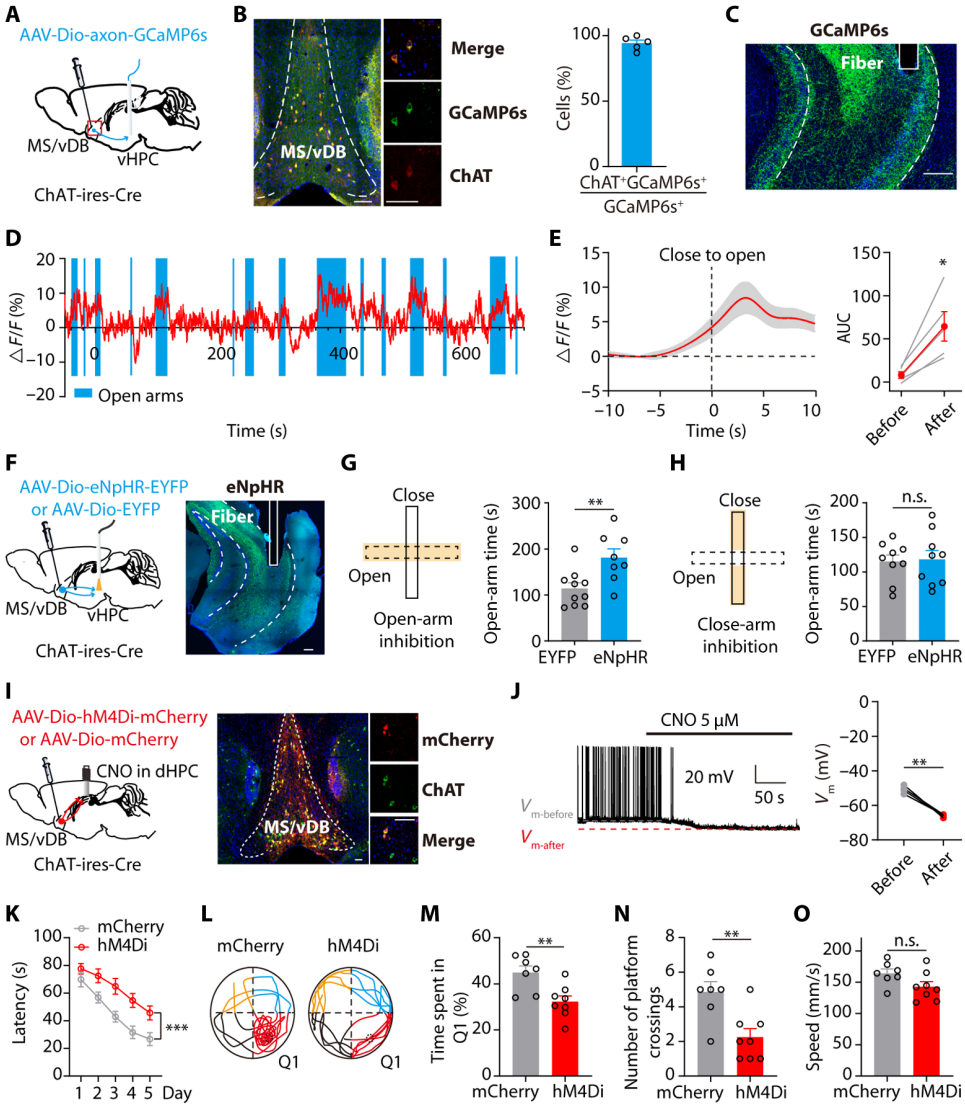

Fig. 5. MS/vDB cholinergic input to the vHPC and the dHPC separately modulates the anxiety-like behavior and spatial learning. (**A**) Recording of the MS/vDB-vHPC cholinergic projections. (**B**) (Left) GCaMP6s expression in the MS/vDB. Scale bar, 100 μm. (Middle) Overlap between GCaMP6s-expressing cells (green) and anti–ChAT-positive cells (red). Scale bar, 20 μm. (Right) Percentage of GCaMP6s$^+$ neurons coexpressing ChAT ($n = 5$ mice). (**C**) Placement of fiber optics. Scale bar, 200 μm. (**D**) Example of vCA1 cholinergic fiber activity. (**E**) Plot of Ca^{2+} transients across animals aligned to the start of open-arm entry and the change in Ca^{2+} signals. $n = 8$. (**F**) Optogenetic silencing of MS/vDB-vHPC cholinergic projections. Scale bar, 200 μm. (**G** and **H**) Open-arm silencing increased the time spent exploring the open arms [(G) EYFP, $n = 10$; eNpHR, $n = 8$]; silencing in the closed arms had no effect [(H) EYFP, $n = 9$; eNpHR, $n = 9$]. (**I**) Chemogenetic inhibition of the MS/vDB-dHPC cholinergic projections [hM4Di (red) and ChAT neurons (green)]. Scale bar, 100 μm. (**J**) Representative trace and summarized data showing the inhibition of hM4Di cells after 5 μM CNO delivery. $n = 4$. (**K**) Escape latency during acquisition training. mCherry, $n = 7$; hM4Di, $n = 8$. (**L**) Representative swimming traces in the probe trial. (**M**) Time spent in Q1. (**N**) Number of platform crossings. (**O**) Speed in the MWM. Paired t test for (E) and (J); unpaired t test for (G), (H), (M), (N), and (O); two-way, repeated-measures ANOVA for (K). $^*P < 0.05$; $^{**}P < 0.01$; $^{***}P < 0.001$. Data are presented as the means ± SEM.

vDB-vHPC cholinergic pathways (figs. S8 and S15F). Together, these observations indicate that MS/vDB cholinergic input to the vHPC regions modulates anxiety-like behaviors via releasing ACh.

We also observed the activity of MS/vDB-dHPC cholinergic fibers (fig. S9A). While acute and severe stressors such as footshock and social attack notably increased the Ca^{2+} signal of MS/vDB-dHPC cholinergic projections (fig. S9, B and C), little enhancement was observed during open-arm entries (fig. S9, D and E), and sucrose reward did not affect the activity of these projections (fig. S9F). In addition, the activation of MS/vDB-dHPC cholinergic terminals did not affect the release of CORT in mice (figs. S9, G and H, and S15G). Optogenetic modulation of MS/vDB-dHPC cholinergic projections did not induce place aversion or anxiety-related behaviors (figs. S9, I to P, and S15H). These findings suggest that the activation of cholinergic projections from the MS/vDB-dHPC may contribute only to the transformation of salient sensory cues but not to emotional valence processing.

Given the well-established involvement of the dHPC region in spatial learning, we sought to investigate the potential role of cholinergic projections from the MS/vDB-dHPC in this process. We used chemogenetic inhibition of the cholinergic projection from the MS/vDB-dHPC via designer receptors exclusively activated by designer drugs (DREADDS) (Fig. 5I). The application of clozapine-N-oxide (CNO, 5 μM) resulted in hyperpolarization and reduction in firing activity among cholinergic neurons (Fig. 5J). The spatial learning and memory of mice were evaluated using the Morris water maze (MWM). During the training session, bilateral injections of CNO were administered into the dHPC region 30 min prior to training. The escape latency was prolonged in mice expressing hM4Di (inhibitory designer receptors exclusively activated by CNO) compared to control mice when reaching the hidden platform (Fig. 5K), indicating impaired spatial learning due to inhibition of MS/vDB-dHPC cholinergic projections. On the sixth day, the proportion of time spent in the target quadrant and the number of target crossings were higher in control mice than in hM4Di-expressing mice (Fig. 5, L to N). In addition, there were no differences in swimming speed between the control group and mice expressing hM4Di (Fig. 5O), indicating no locomotor impairment. In contrast, using the identical strategy yielded no indication of MS/vDB-vHPC cholinergic projections involved in spatial learning processes (figs. S10 and S15I). Together, these results of circuit modulation suggest that the cholinergic projections of the MS/vDB-vHPC and MS/vDB-dHPC can independently mediate anxiety-like behaviors and spatial learning.

ChAT$^{MS/vDB\text{-}dHPC}$ and ChAT$^{MS/vDB\text{-}vHPC}$ neurons exhibit distinct electrophysiological and transcriptional adaptations following chronic restraint stress

Previous research has demonstrated that chronic stress can lead to both cognitive dysfunction and emotional disorders (*49*, *50*). Consistently, our findings demonstrate that mice exposed to chronic restraint stress exhibit elevated levels of anxiety (fig. S11, A to E) and impaired spatial learning and memory (fig. S11, F to J). The acute restraint stress led to an increase in ACh release in the vHPC while causing a decrease in ACh release in the dHPC (fig. S12). Hence, we investigated if the activity of ChAT$^{MS/vDB\text{-}dHPC}$ and ChAT$^{MS/vDB\text{-}vHPC}$ neurons was altered under pathological stress. The mice were divided into two groups: One group was subjected to chronic restraint stress, while the other received 5 min of gentle handling. Subsequently, the targeted neurons were examined via whole-cell patch-clamp recordings (Fig. 6A). We observed a notable increase in the firing activity of ChAT$^{MS/vDB\text{-}vHPC}$ neurons evoked by depolarization in stress mice (Fig. 6B). Using the same approach, we demonstrated that chronic stress impaired the intrinsic excitability of ChAT$^{MS/vDB\text{-}dHPC}$ neurons (Fig. 6, C and D). Overall, our electrophysiological findings demonstrate that animals subjected to chronic stress exhibit enhanced ChAT$^{MS/vDB\text{-}vHPC}$ neuronal activity and reduced ChAT$^{MS/vDB\text{-}dHPC}$ neuronal activity.

We next attempted to gain insights into the transcriptional adaptation of ChAT$^{MS/vDB\text{-}dHPC}$ and ChAT$^{MS/vDB\text{-}vHPC}$ neurons following chronic stress. Following stress, individual neurons were aspirated using pipettes (Fig. 6E). Labeling and sorting ChAT$^{MS/vDB\text{-}dHPC}$ and ChAT$^{MS/vDB\text{-}vHPC}$ neurons from the mice are described in detail in Materials and Methods. RNA sequencing (RNA-seq) libraries were established from each population and profiled by Illumina high-throughput RNA-seq.

To elucidate the electrophysiological phenotypes of ChAT$^{MS/vDB\text{-}dHPC}$ and ChAT$^{MS/vDB\text{-}vHPC}$ neurons under both physiological and pathological conditions, our primary focus was on the expression of ion channel genes. We applied a cutoff of at least twofold and a P value of <0.05 to score the gene expression profiles. RNA-seq analysis revealed that *Scn5a*, which belongs to a family of genes that provide instructions for making sodium channel Nav1.5, was highly expressed in ChAT$^{MS/vDB\text{-}dHPC}$ neurons, while *Cacna2d4* and *Cacna1h*, which belong to genes that provide instructions for making the voltage-dependent calcium channels, were highly expressed in ChAT$^{MS/vDB\text{-}vHPC}$ neurons (Fig. 6F). Although previous studies identified higher expression of several molecules, including serotonin1A receptors, in a subpopulation of cholinergic neurons within the septal region (*24*, *34*, *35*), there was no difference in the mRNA expression of these molecules between ChAT$^{MS/vDB\text{-}dHPC}$ neurons and ChAT$^{MS/vDB\text{-}vHPC}$ neurons (fig. S13).

Following chronic stress, in ChAT$^{MS/vDB\text{-}dHPC}$ neurons, eight ion channel genes were up-regulated, and five ion channel genes were down-regulated. Among them, *Scn5a*, which was highly expressed in ChAT$^{MS/vDB\text{-}dHPC}$ but not ChAT$^{MS/vDB\text{-}vHPC}$ neurons, was greatly down-regulated after stress (Fig. 6G). For ChAT$^{MS/vDB\text{-}vHPC}$ neurons, only 1 ion channel gene, *Clcn1* (a gene related to voltage-gated chloride channels), was down-regulated, while 19 ion channel genes were up-regulated, such as *Scn1a* and *Scn1b*, genes coding for voltage-gated sodium channels (Fig. 6H). These observations suggest that the mechanisms underlying electrophysiological changes after chronic stress may involve differentially expressed candidate ion channel genes.

Together with the aforementioned optogenetic and chemogenetic data in naïve mice (Fig. 5), the contrasting alterations observed in these two subpopulations of neurons may differentially contribute to distinct symptoms induced by chronic stress.

Modulating discrete septo-hippocampal cholinergic circuits rescues stress-induced symptoms

To further investigate if the hyperactivity of ChAT$^{MS/vDB\text{-}vHPC}$ neurons and sluggishness of ChAT$^{MS/vDB\text{-}dHPC}$ neurons induced by chronic stress separately contribute to elevated anxiety and cognitive impairments, we chemogenetically antagonize the alterations in these two pathways. To achieve this, we initially expressed hM3Dq (excitatory designer receptors exclusively activated by CNO) or control virus in MS/vDB ChAT neurons and implanted cannulas above the dHPC (Fig. 7A and fig. S15C). Subsequently, the mice were subjected to stress. After stress, both stressed and control mice were subjected to behavioral assays, with bilateral delivery of CNO into the dHPC region 30 min prior to the tests (Fig. 7B). As anticipated, the chemogenetic activation of MS/vDB-dHPC cholinergic projections mitigated the decline in spatial learning and memory observed in the MWM (Fig. 7, C to F). On the other hand, the inhibition of MS/vDB-vHPC cholinergic projections by hM4Di reversed the anxiety-like behaviors induced by stress, as evidenced by a notable increase in center time during the OFT and open-arm time in the EPM (Fig. 7, G to K, and fig. S15D).

These data indicate that it is probable that the aberrant activity of distinct septo-hippocampal cholinergic circuits induced by chronic stress separately modulates emotional and cognitive impairments.

AChEIs combined with blockade of the M1 ameliorate both cognitive deficits and anxiety-like behaviors in stressed mice

We next investigated if stress-induced behavioral deficits could be rescued by targeting circuit-based cholinergic signaling pathways.

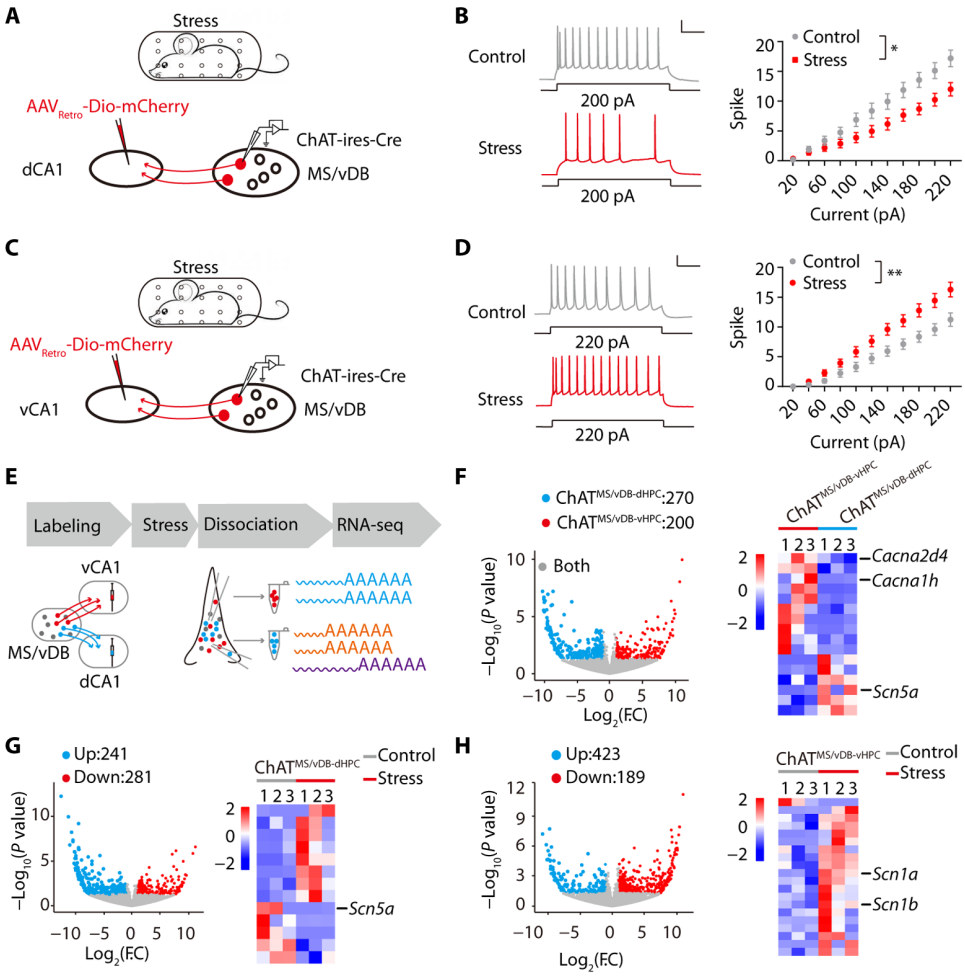

Fig. 6. ChAT$^{MS/vDB\text{-}dHPC}$ and ChAT$^{MS/vDB\text{-}vHPC}$ neurons exhibit distinct electrophysiological and transcriptional adaptations to chronic restraint stress. (**A**) Schematic of chronic restraint stress and recording of ChAT$^{MS/vDB\text{-}dHPC}$ neurons. (**B**) (Left) Representative traces. Scale bar, 100 ms, 20 mV. (Right) Injected current-evoked firing relationship of ChAT$^{MS/vDB\text{-}dHPC}$ neurons. Control, $n = 15$; stress, $n = 15$. (**C**) Schematic of chronic restraint stress and recording of ChAT$^{MS/vDB\text{-}vHPC}$ neurons. (**D**) (Left) Representative traces. Scale bar, 100 ms, 20 mV. (Right) Injected current-evoked firing relationship of ChAT$^{MS/vDB\text{-}vHPC}$ neurons. Control, $n = 14$; stress, $n = 15$. (**E**) Strategy of neuronal type–specific RNA-seq. (**F**) (Left) Scatterplots showing the genes enriched in ChAT$^{MS/vDB\text{-}vHPC}$ (red) versus ChAT$^{MS/vDB\text{-}dHPC}$ (green) neurons and both (gray). (Right) Heatmap showing ChAT$^{MS/vDB\text{-}dHPC}$ and ChAT$^{MS/vDB\text{-}vHPC}$ neuron-enriched ion channel-related genes. F.C, fold change. (**G**) (Left) Scatterplots showing the genes down-regulated (red) versus up-regulated (green) in ChAT$^{MS/vDB\text{-}dHPC}$ neurons after chronic stress. (Right) Heatmap showing ion channel-related genes in ChAT$^{MS/vDB\text{-}dHPC}$ neurons with a notable change after chronic stress. (**H**) (Left) Scatterplots showing the genes down-regulated (red) versus up-regulated (green) in ChAT$^{MS/vDB\text{-}vHPC}$ neurons after chronic stress. (Right) Heatmap showing ion channel-related genes in ChAT$^{MS/vDB\text{-}vHPC}$ neurons with a notable change after chronic stress. Two-way, repeated-measures ANOVA for (B) and (D). $^{*}P < 0.05$; $^{**}P < 0.01$. Data are presented as the means ± SEM.

Single-cell transcriptomics analysis of the entire mouse hippocampal formation reveals distinct expression patterns of ACh receptors in the dCA1 and vCA1 regions, with widespread expression of M1 and M3 (*51*). The ISH (in situ hybridization) database of the Allen Brain Atlas shows a high expression level of the M1 gene in both the dCA1 and vCA1 regions, whereas the M3 gene was scarcely expressed in the vCA1 (fig. S14A). Then, we specifically expressed ChR2 in the cholinergic fibers from the MS/vDB to the dCA1 or vCA1 to examine the contribution of M1 and M3 receptors to synaptic transmission mediated by these two projections with whole-cell patch-clamp recording (Fig. 8, A and C). Light-induced ACh release evoked nicotinic inward currents (fast-currents, F-currents) and muscarinic inward currents (slow-currents, S-currents) in both dCA1 and vCA1 pyramidal cells (Fig. 8, B and D), which were separately dependent on nAChRs and mAChRs (*48*, *52*). In the vCA1 region, the M1 receptor inhibitor (M1i) but not the M3 receptor inhibitor (M3i) suppressed light-induced muscarinic inward currents (Fig. 8B). In the dCA1 region, the muscarinic inward currents could be suppressed by either M3i or M1i (Fig. 8D). These observations suggest that the M1 receptors are essential for the MS/vDB-vHPC cholinergic pathway, whereas the postsynaptic excitatory effect of the dCA1 cholinergic projection is mediated by both M1 and M3 receptors.

Multiple lines of evidence suggest that AChEIs are effective in treating cognitive deficits associated with neurodegenerative diseases by elevating ACh levels (*53*, *54*). However, numerous clinical and animal studies have demonstrated that acute administration of AChEIs results in increases in plasma cortisol levels and induces high levels of anxiety (*38*, *40*, *42*, *55*), which may exacerbate the anxiety state of

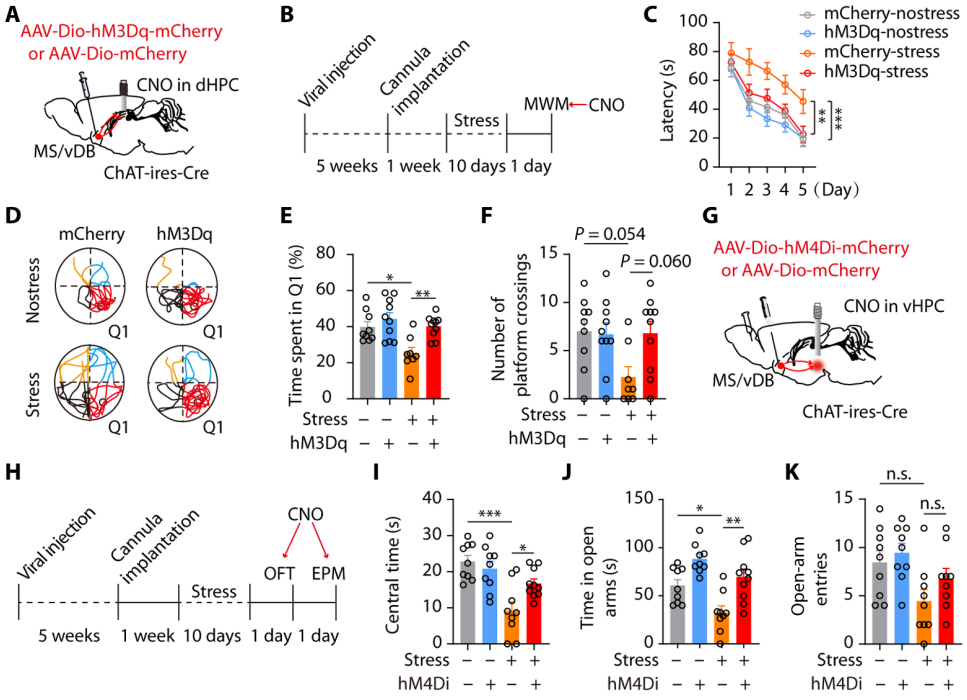

Fig. 7. Manipulating different septo-hippocampal cholinergic pathways can rescue memory deficits and anxiety-like behaviors induced by chronic stress. (**A**) Chemogenetic activation of the MS/vDB-dHPC cholinergic projections. (**B**) Timeline of experiments. (**C**) Escape latency during acquisition training. mCherry-nostress, $n = 9$; hM3Dq-nostress, $n = 10$; mCherry-stress, $n = 8$; hM3Dq-stress, $n = 10$. (**D**) Representative traces of swimming paths in the probe trial. (**E**) Time spent in Q1. (**F**) Number of platform crossings. (**G**) Schematic for injection of hM4Di and control virus in MS/vDB and CNO delivery in the vHPC. (**H**) Timeline of experiments. (**I**) Time spent in the center in stressed mice. mCherry-nostress, $n = 9$; hM4Di-nostress, $n = 9$; mCherry-stress, $n = 9$; hM4Di-stress $n = 10$. (**J**) Time spent in the open arms. (**K**) Open-arm entries. Two-way, repeated-measures ANOVA with Tukey's multiple comparisons test (C) and one-way ANOVA with Tukey's multiple comparisons test [(E), (F), and (I) to (K)]. $^{*}P < 0.05$; $^{**}P < 0.01$; $^{***}P < 0.001$. Data are presented as the means ± SEM.

stressed mice. Given that increased ACh release in the vCA1 region modulates neuronal activity via M1 receptors, we first investigated if blocking vHPC M1 receptors can attenuate the emotional impact of acute AChEI administration. We intraperitoneally injected donepezil, a clinically used AChEI, at a dose of 1.0 mg/kg into male mice (*56*, *57*) with artificial cerebrospinal fluid (ACSF) or M1 inhibitor (M1i) intra-vCA1 injection. Control mice were administered intraperitoneally with saline and received local injections of ACSF into the vHPC region (fig. S14B). The results showed that administration of donepezil induced anxiogenic effects in the OFT and EPM; these effects were abolished by local blockade of M1 receptors in the vHPC region (fig. S14, C and D). These findings suggest that the activation of local M1 receptors by ACh underlies the mechanism for donepezil-induced anxiety-like behaviors.

We next investigated if the combination of donepezil and M1i could ameliorate both cognitive and emotional impairments in stressed mice (Fig. 8E). In the EPM test, we observed that administration of donepezil in stressed mice exacerbated their anxiety state. However, delivery of M1i into the vHPC alone or in combination with donepezil effectively ameliorated the anxiety-like behavior in stressed mice (Fig. 8, F and G). In the MWM test, administration of donepezil alone or in combination with M1i ameliorated stress-induced cognitive impairment; however, no improvement was observed in the stress group that received M1i infusion into the vHPC region (Fig. 8, H to K). Therefore, these results demonstrate that the combined delivery of donepezil and M1i could effectively reverse emotional and cognitive deficits induced by chronic stress.

DISCUSSION

Studies on patients suffering from chronic stress have traditionally focused on emotional symptoms. However, poorly controlled cognitive deficits are equally prominent and severely compromise quality of life (*58*). Few studies have systematically approached the understanding of potential circuits underlying emotional and cognitive deficits in these patients. In this study, we identified two distinct septo-hippocampal cholinergic circuits in mice that are responsible for cognitive and emotional deficits under chronic stress conditions. Furthermore, by targeting circuit-based cholinergic signaling pathways, we effectively rescued these stress-induced deficits in mice, providing a promising strategy for treating emotional and cognitive deficits in stress-related psychiatric disorders.

Previous research has indicated that over 50% of MS neurons are activated by aversive stimuli originating from various peripheral regions (*22*). A recent study indicated that aversive sensory stimuli activate glutamatergic neurons in the MS while inhibiting GABAergic neurons (*11*). However, the response of MS/vDB ChAT neurons to aversive stimuli or rewards remains poorly understood. Previous studies demonstrated that stress induced increasing in ACh levels within the dHPC or vHPC (*59*–*61*). Consistently, we found the activation of both MS/vDB-dHPC and MS/vDB-vHPC cholinergic projections after footshock. However, we observed two distinct projections exhibiting differential activities in response to diverse stimuli. $ChAT^{MS/vDB\text{-}dHPC}$ neurons are exclusively activated by intense aversive stimuli, such as footshock and social attack, while relatively mild aversive stimuli (open arms) or rewards have no impact on their activity. A similar study

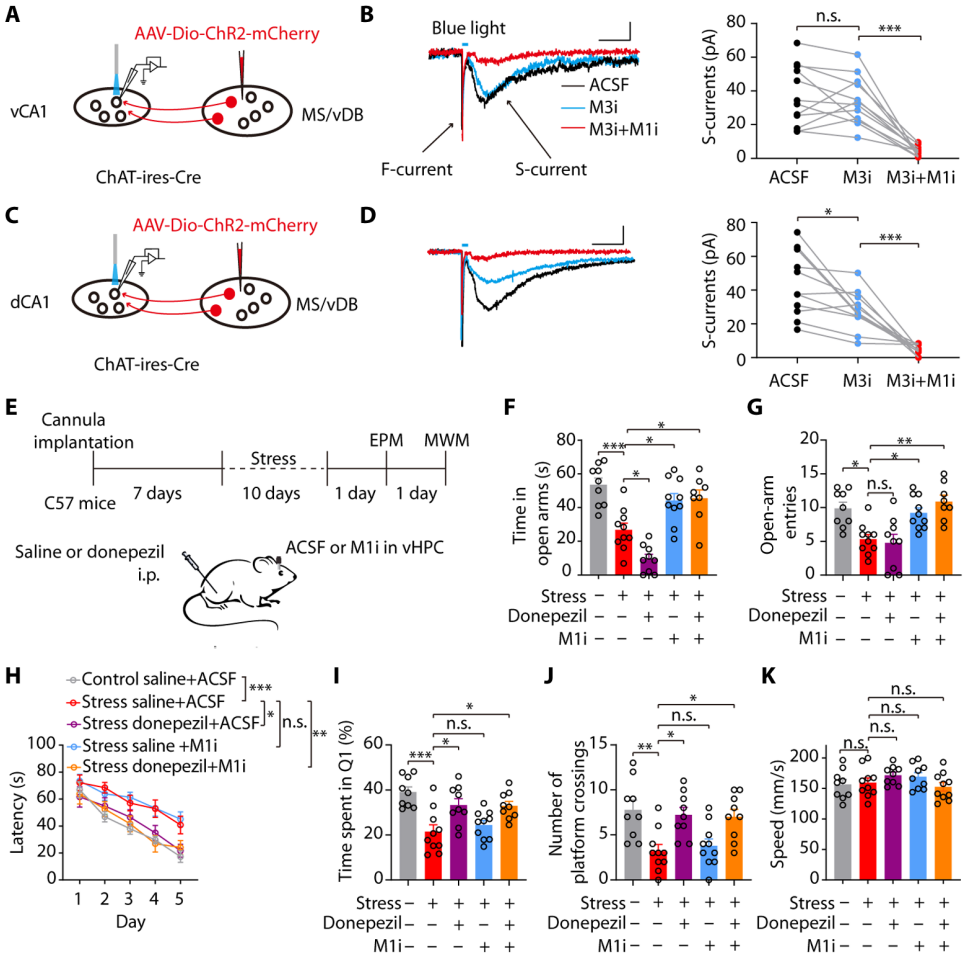

Fig. 8. AChEIs combined with blockade of the M1 receptor ameliorate both cognitive deficits and anxiety-like behaviors in stressed mice. (**A** and **C**) Schematic of viral injection, the location of light stimuli, and the recording configuration in acute slices. (**B**) Representative traces (left) and quantification (right) show light-evoked muscarinic inward currents were suppressed by application of the M3 inhibitor DAU5884 (M3i; 5 μM) but not the M1 inhibitor VU0255035 (M1i; 5 μM). Scale bar, 100 ms, 20 pA ($n = 12$ neurons from four mice). (**D**) Representative traces (left) and quantification (right) show muscarinic inward currents were suppressed by application of M3i or M1i. Scale bar, 100 ms, 20 pA ($n = 11$ neurons from four mice). (**E**) Timeline of experiments and scheme of drug delivery strategy. (**F** and **G**) Time spent in the open arms [(F) $n = 8$ to 10) and open-arm entries (G). (**H**) Donepezil injection combined with intra-vHPC delivery of M1i in stress mice during the training session reversed the impairment of spatial learning in the MWM. (**I** to **K**) Donepezil injection combined with intra-vHPC delivery of M1i during the training session in stressed mice increased the time spent in Q1 (I) and the number of platform crossings (J) with no effect on speed (K). One-way ANOVA with Tukey's multiple comparison test for (B) and (D) and two-way ANOVA with Bonferroni's multiple comparison test for (F), (G), (I), (J), and (K). *$P < 0.05$; **$P < 0.01$; ***$P < 0.001$. Data are presented as the means ± SEM.

demonstrated that the cholinergic fibers of the MS/vDB-dHPC exhibit increased activity solely in response to air puff stimulation and display minimal responsiveness to light flashes or tone stimuli (*62*). Furthermore, the activation of MS/vDB-dHPC cholinergic projections did not elicit any emotional response in mice. Our hypothesis posits that $ChAT^{MS/vDB\text{-}dHPC}$ neurons only transform salient sensory cues, thereby serving as a gate for relaying salient signals to facilitate cognitive function. This pattern can prevent the body from developing hypersensitivity to insignificant external stimuli. Previous MS single-unit in vivo recording revealed a similar response, indicating that noise stimuli are more effective than pure tones in driving MS neurons with a moderate intensity threshold (*63*). Notably, we have also found that $ChAT^{MS/vDB\text{-}vHPC}$ neurons respond to a broad spectrum of stimuli. These neurons exhibit rapid, biphasic responses that encode the positive and negative valences of stimuli as they are promptly activated by aversive cues and inhibited by appetitive stimuli. However, other studies have indicated that both appetitive rewards and aversive stimuli elicit the activation of ChAT neurons in the basal forebrain (*44*–*46*, *64*). It should be noticed that the ChAT neurons recording in these studies are predominantly from the hDB, another subregion of the basal forebrain. The ChAT neurons in the hDB are anatomically distinct with those ChAT neurons in the MS/vDB recorded in our study (*5*). Moreover, our observation of inhibiting ChAT neurons in the MS/vDB in response to reward may be attributed to the activation of GABAergic neurons in the MS/vDB (*65*). These divergent findings indicate functional heterogeneity among cholinergic neurons in subregions of the basal forebrain.

Our anterograde and retrograde tracing indicated that $ChAT^{MS/vDB\text{-}dHPC}$ and $ChAT^{MS/vDB\text{-}vHPC}$ neurons are distinct subpopulations, which is consistent with previous findings demonstrating differences in the projection patterns of adjacent basal forebrain neurons (*47*). Furthermore, studies have indicated that several receptors, including serotonin and CRF receptors, exhibit different expression among

MS ChAT neurons (*34*, *35*, *66*). A more recent study has demonstrated that MS ChAT neurons, which express either calbindin-D28K or not, project to the vCA1 and dDG regions, exhibiting distinct functional characteristics in regulating the anxiety-like behavior and spatial learning (*48*). In addition to the similar findings, our study has further recorded the neuronal activity of ChAT neurons and their distinct projections under diverse stimuli, which help to precisely clarify how neurons contribute to information processing. External information can be detected, interpreted, evaluated, and responded to by succeeding levels of highly interconnected neural circuits (*67*). The amygdala complex is recognized as a key region involved in the interpretation of sensory information as it assigns valence to different primary information (*68*). Therefore, our recorded findings of MS/vDB-dHPC cholinergic projections in processing salient stimuli and MS/vDB-vHPC cholinergic projections in processing positive and negative valence highlight the pivotal role of the MS/vDB region as another crucial hub in interpreting external information. Combined with the manipulation evidence, these findings further support a substantial involvement of cholinergic neurons in the interpretation of sensory information within the MS/vDB.

We identified a precise input organization of subpopulations of ChAT neurons in the MS/vDB. Our findings reveal that ChAT$^{MS/vDB\text{-}dHPC}$ neurons are predominantly targeted by neurons located in the subiculum and LEnT regions. The subiculum is known to play a crucial role in spatial processing (*69*, *70*), while the LEnT is engaged in the process of associative memory (*71*, *72*). These two regions may transmit information to ChAT$^{MS/vDB\text{-}dHPC}$ neurons to facilitate their role in spatial memory function. In contrast, ChAT$^{MS/vDB\text{-}vHPC}$ neurons exhibited a higher degree of innervation from the ARC, LH, and DRN. The ARC is renowned for its role in modulating feeding behaviors, with Agouti-related protein and proopiomelanocortin-positive cells within the ARC being activated during appetitive reward (*73*, *74*). Sucrose reward could potentially alleviate stress (*75*); the association between ARC and ChAT$^{MS/vDB\text{-}vHPC}$ neurons may account for the appetite-induced suppression of ChAT$^{MS/vDB\text{-}vHPC}$ neuronal activities. However, further research is required to elucidate the underlying mechanisms of ChAT$^{MS/vDB\text{-}vHPC}$ neuronal activity inhibition during appetitive reward. Furthermore, the stress-induced activation of neurons in the LH region is responsible for encoding negative valence (*76*, *77*). Therefore, ChAT$^{MS/vDB\text{-}vHPC}$ neurons are capable of integrating negative valence signals from the LH and projecting directly to vCA1 neurons, thereby eliciting avoidant behaviors. It is necessary to further investigate the upstream inputs of ChAT$^{MS/vDB\text{-}vHPC}$ neurons implicated in the modulation of anxiety-like behaviors.

The findings of our study suggest that distinct cholinergic projections to the hippocampus modulate cognitive function and anxiety states in mice. Theta rhythm in the hippocampus has been linked to both cognitive and emotional functions. It has been shown that spatial memory performance is positively correlated with the theta power in the dHPC, and restoration of theta-like rhythmicity can restore lost cognitive function (*78*, *79*). Meanwhile, mice avoidance behaviors are accompanied with increased theta power in the vHPC (*80*), and anxiolytic drugs can decrease the hippocampal theta frequency (*81*, *82*). Cholinergic regulation of hippocampal theta rhythm has been proposed as one of the central mechanisms underlying hippocampal functions including spatial memory encoding (*83*, *84*). Further works are needed to investigate the impact of distinct cholinergic subtypes on theta rhythm in the dHPC and vHPC.

We observed distinct electrophysiological adaptations in ChAT$^{MS/vDB\text{-}dHPC}$ and ChAT$^{MS/vDB\text{-}vHPC}$ neurons under chronic stress conditions. The differential molecular expression between ChAT$^{MS/vDB\text{-}dHPC}$ and ChAT$^{MS/vDB\text{-}vHPC}$ neurons following chronic stress may account for their distinct neuronal adaptations. In this study, we demonstrate that *Scn5a* is selectively expressed in ChAT$^{MS/vDB\text{-}dHPC}$ neurons but not ChAT$^{MS/vDB\text{-}vHPC}$ neurons. Following chronic stress, there is a significant reduction in *Scn5a* expression, which may contribute to the decreased excitability of ChAT$^{MS/vDB\text{-}dHPC}$ neurons. *Scn5a* mutations are linked to human cardiac long QT syndrome and ventricular fibrillation; however, their role in mental disease remains unknown (*85*). Furthermore, *Scn1a*, coding for the voltage-gated sodium channel Nav1.1, was up-regulated in ChAT$^{MS/vDB\text{-}vHPC}$ neurons after stress. The enhanced expression of *Scn1a* may result in the increased excitability of ChAT$^{MSDB\text{-}vHPC}$ neurons. A previous study indicated the wide expression of Nav1.1 in MS/vDB ChAT neurons (*86*). In addition, knockout of *Scn1a* in the brain could decrease animals' anxiety levels (*87*, *88*). Further research is necessary to determine the molecular contribution to the excitability of the two subtypes of ChAT neurons, which could facilitate targeted treatment of specific symptoms associated with chronic stress within neural circuits. Alternatively, as assessed in our experiments, the differential neuronal adaptations between ChAT$^{MS/vDB\text{-}dHPC}$ and ChAT$^{MS/vDB\text{-}vHPC}$ populations may be partially attributed to the distinct input patterns observed in each population.

Our electrophysiological findings demonstrate a reduction in the excitability of ChAT$^{MS/vDB\text{-}dHPC}$ neurons following chronic stress, which is consistent with previous research indicating that chronic stress leads to decreased ACh levels in the dHPC (*89*). Furthermore, the activation of ChAT$^{MS/vDB\text{-}dHPC}$ neurons through chemogenetics or donepezil injection can effectively ameliorate cognitive deficits induced by stress. Similar with our findings, previous research has demonstrated that donepezil can mitigate stress-induced cognitive inflexibility in rats (*90*). Enhancing cholinergic signaling appears to be a promising strategy for alleviating cognitive impairment induced by chronic stress.

ChAT$^{MS/vDB\text{-}vHPC}$ neurons exhibit hyperexcitability following exposure to chronic stress, which is consistent with previous findings of increased ACh levels in the vCA1 region under chronic stress conditions (*91*, *92*). The vHPC plays a pivotal role in the neural circuit mediating negative affective behaviors, whereby the activation of vCA1 cell bodies and their projections can bidirectionally modulate anxiety-like behaviors (*93*, *94*). However, the precise mechanisms by which neuromodulators regulate behaviors in the vHPC remain poorly understood. We demonstrate that targeted manipulation of the cholinergic projection from the MS/vDB-vHPC modulates anxiety levels in naïve mice. Moreover, the inhibition of this neural pathway effectively reversed the anxiety-like behaviors induced by stress, indicating a crucial role of this projection in the pathogenesis of anxiety disorders.

The hippocampal dorsoventral axis is functionally segregated into the dorsal part that is essential for visuospatial information processing, the ventral part that is involved in emotional, motivational, and affective responses, and the intermediate part that integrates information from both poles (*95*–*98*). The cholinergic projections originating from the MS/vDB innervate to the whole hippocampal formation (*47*). It remains uncertain if dCA1-projecting or vCA1-projecting MS/vDB ChAT neurons can also innervate the intermediate CA1 region or if there are specific MS/vDB neurons that target

the intermediate CA1 region. Meanwhile, what is the function of the cells projecting to intermediate CA1 during chronic restraint stress requires further investigation.

Although AChEIs are now considered a first-line treatment for cognitive deficits, their acute use may exacerbate emotional symptoms and lead to poor therapeutic compliance for stress-related disorders. Our findings strongly suggest that the engagement of M1 receptors in vCA1 by acute AChEIs induces aversive behaviors in rodents, which could potentially explain early adverse events observed in clinical populations. Therefore, it is crucial to identify compounds that exhibit selectivity toward circuit-specific cellular populations.

In summary, by targeting circuit-based cholinergic signaling pathways, we can ameliorate the stress-induced emotional and cognitive disorders. These findings may offer insights into the development of circuit-specific treatments for stress-related disorders. Moreover, the invasive modulation of cholinergic circuits in our study necessitates further investigation into pharmacologically targeting different ACh receptors in the dHPC and vHPC for the treatment of stress-related emotional and cognitive deficits.

MATERIALS AND METHODS

We used (all males, aged 8 to 12 weeks) ChAT-ires-Cre mice (Jax no. 006410, a gift from L. Xiaoming at Zhejiang University). Male C57BL/6J mice (aged 8 to 10 weeks) were obtained from the Southern Medical University Animal Center (Guangzhou, China). Ethics approval for this study was obtained from the ethics board for animal research at the Southern Medical University (Animal Welfare Assurance no. D2022111). The procedures used for virus construction and packaging, virus injection, optical fiber and guide cannula placement, retrograde labeling, electrophysiological recordings, light delivery, drug delivery, behavioral assays, histology, and imaging are detailed in the Supplementary Materials.

Statistics

We conducted simple statistical comparisons using Student's t test. Analysis of variance (ANOVA) (one-way and two-way) and post hoc analyses were used to statistically analyze the data from the experimental groups with multiple comparisons. All statistical analyses were performed using the GraphPad Prism 8 software. All significant statistical results are indicated on the figures following the conventions: $^{*}P < 0.05$; $^{**}P < 0.01$; $^{***}P < 0.001$. All data are presented as the means ± SEM.

Supplementary Materials

This PDF file includes:

Supplementary Materials and methods
Figs. S1 to S15

REFERENCES AND NOTES

1. B. S. McEwen, N. P. Bowles, J. D. Gray, M. N. Hill, R. G. Hunter, I. N. Karatsoreos, C. Nasca, Mechanisms of stress in the brain. *Nat. Neurosci.* **18**, 1353–1363 (2015).
2. R. J. Fenster, L. A. M. Lebois, K. J. Ressler, J. Suh, Brain circuit dysfunction in post-traumatic stress disorder: From mouse to man. *Nat. Rev. Neurosci.* **19**, 535–551 (2018).
3. L. Schwabe, E. J. Hermans, M. Joëls, B. Roozendaal, Mechanisms of memory under stress. *Neuron* **110**, 1450–1467 (2022).
4. D. de Quervain, L. Schwabe, B. Roozendaal, Stress, glucocorticoids and memory: Implications for treating fear-related disorders. *Nat. Rev. Neurosci.* **18**, 7–19 (2017).
5. E. C. Ballinger, M. Ananth, D. A. Talmage, L. W. Role, Basal forebrain cholinergic circuits and signaling in cognition and cognitive decline. *Neuron* **91**, 1199–1218 (2016).
6. C. Muller, S. Remy, Septo-hippocampal interaction. *Cell Tissue Res.* **373**, 565–575 (2018).
7. X. Wu, W. Morishita, K. T. Beier, B. D. Heifets, R. C. Malenka, 5-HT modulation of a medial septal circuit tunes social memory stability. *Nature* **599**, 96–101 (2021).
8. R. Boyce, S. D. Glasgow, S. Williams, A. Adamantidis, Causal evidence for the role of REM sleep theta rhythm in contextual memory consolidation. *Science* **352**, 812–816 (2016).
9. A. Sans-Dublanc, A. Razzauti, S. Desikan, M. Pascual, H. Monyer, C. Sindreu, Septal GABAergic inputs to CA1 govern contextual memory retrieval. *Sci. Adv.* **6**, eaba5003 (2020).
10. A. Degroot, D. Treit, Anxiety is functionally segregated within the septo-hippocampal system. *Brain Res.* **1001**, 60–71 (2004).
11. G.-W. Zhang, L. Shen, W. Zhong, Y. Xiong, L. I. Zhang, H. W. Tao, Transforming sensory cues into aversive emotion via septal-habenular pathway. *Neuron* **99**, 1016–1028.e5 (2018).
12. N. Yu, H. Song, G. Chu, X. Zhan, B. Liu, Y. Mu, J.-Z. Wang, Y. Lu, Basal forebrain cholinergic innervation induces depression-like behaviors through ventral subiculum hyperactivation. *Neurosci. Bull.* **39**, 617–630 (2023).
13. S. T. Ang, M. Z. Ariffin, S. Khanna, The forebrain medial septal region and nociception. *Neurobiol. Learn. Mem.* **138**, 238–251 (2017).
14. Z. Zheng, C. Guo, M. Li, L. Yang, P. Liu, X. Zhang, Y. Liu, X. Guo, S. Cao, Y. Dong, C. Zhang, M. Chen, J. Xu, H. Hu, Y. Cui, Hypothalamus-habenula potentiation encodes chronic stress experience and drives depression onset. *Neuron* **110**, 1400–1415.e6 (2022).
15. P. Tovote, M. S. Esposito, P. Botta, F. Chaudun, J. P. Fadok, M. Markovic, S. B. E. Wolff, C. Ramakrishnan, L. Fenno, K. Deisseroth, C. Herry, S. Arber, A. Lüthi, Midbrain circuits for defensive behaviour. *Nature* **534**, 206–212 (2016).
16. K. Martinowich, K. M. Cardinale, R. J. Schloesser, M. Hsu, N. H. Greig, H. K. Manji, Acetylcholinesterase inhibition ameliorates deficits in motivational drive. *Behav. Brain Funct.* **8**, 15 (2012).
17. J. T. McKenna, J. W. Cordeira, B. A. Jeffrey, C. P. Ward, S. Winston, R. W. McCarley, R. E. Strecker, c-Fos protein expression is increased in cholinergic neurons of the rodent basal forebrain during spontaneous and induced wakefulness. *Brain Res. Bull.* **80**, 382–388 (2009).
18. Y. M. Ulrich-Lai, J. P. Herman, Neural regulation of endocrine and autonomic stress responses. *Nat. Rev. Neurosci.* **10**, 397–409 (2009).
19. F. R. Calaresu, J. Ciriello, G. J. Mogenson, Identification of pathways mediating cardiovascular responses elicited by stimulation of the septum in the rat. *J. Physiol.* **260**, 515–530 (1976).
20. S. D. Donevan, A. V. Ferguson, Subfornical organ and cardiovascular influences on identified septal neurons. *Am. J. Physiol.* **254**, R544–R551 (1988).
21. L. S. Urzedo-Rodrigues, H. S. Ferreira, D. O. Almeida, J. P. Medeiros, A. Batista, E. de Castro e Silva, J. B. Fregoneze, Blockade of 5-HT3 receptors at septal area increase blood pressure in unanaesthetized rats. *Auton. Neurosci.* **159**, 51–61 (2011).
22. P. Dutar, Y. Lamour, A. Jobert, Activation of identified septo-hippocampal neurons by noxious peripheral stimulation. *Brain Res.* **328**, 15–21 (1985).
23. S. Hupalo, C. A. Bryce, D. A. Bangasser, C. W. Berridge, R. J. Valentino, S. B. Floresco, Corticotropin-Releasing Factor (CRF) circuit modulation of cognition and motivation. *Neurosci. Biobehav. Rev.* **103**, 50–59 (2019).
24. Z. J. Rosinger, J. S. Jacobskind, S. G. Park, N. J. Justice, D. G. Zuloaga, Distribution of corticotropin-releasing factor receptor 1 in the developing mouse forebrain: A novel sex difference revealed in the rostral periventricular hypothalamus. *Neuroscience* **361**, 167–178 (2017).
25. K. R. Wiersielis, A. Ceretti, A. Hall, S. T. Famularo, M. Salvatore, A. S. Ellis, H. Jang, M. E. Wimmer, D. A. Bangasser, Sex differences in corticotropin releasing factor regulation of medial septum-mediated memory formation. *Neurobiol. Stress* **10**, 100150 (2019).
26. P. Dutar, M. H. Bassant, M. C. Senut, Y. Lamour, The septohippocampal pathway: Structure and function of a central cholinergic system. *Physiol. Rev.* **75**, 393–427 (1995).
27. M. Sala, J. Perez, P. Soloff, S. Ucelli di Nemi, E. Caverzasi, J. C. Soares, P. Brambilla, Stress and hippocampal abnormalities in psychiatric disorders. *Eur. Neuropsychopharmacol.* **14**, 393–405 (2004).
28. J. D. Gray, J. F. Kogan, J. Marrocco, B. S. McEwen, Genomic and epigenomic mechanisms of glucocorticoids in the brain. *Nat. Rev. Endocrinol.* **13**, 661–673 (2017).
29. A. Surget, C. Belzung, Adult hippocampal neurogenesis shapes adaptation and improves stress response: A mechanistic and integrative perspective. *Mol. Psychiatry* **27**, 403–421 (2022).
30. H. Zhu, H. Yan, N. Tang, X. Li, P. Pang, H. Li, W. Chen, Y. Guo, S. Shu, Y. Cai, L. Pei, D. Liu, M.-H. Luo, H. Man, Q. Tian, Y. Mu, L.-Q. Zhu, Y. Lu, Impairments of spatial memory in an Alzheimer's disease model via degeneration of hippocampal cholinergic synapses. *Nat. Commun.* **8**, 1676 (2017).
31. D. Mitsushima, A. Sano, T. Takahashi, A cholinergic trigger drives learning-induced plasticity at hippocampal synapses. *Nat. Commun.* **4**, 2760 (2013).
32. D. Pimpinella, V. Mastrorilli, C. Giorgi, S. Coemans, S. Lecca, A. L. Lalive, H. Ostermann, E. C. Fuchs, H. Monyer, A. Mele, E. Cherubini, M. Griguoli, Septal cholinergic input to CA2 hippocampal region controls social novelty discrimination via nicotinic receptor-mediated disinhibition. *eLife* **10**, e65580 (2021).

33. Y. Zhang, Y.-Y. Jiang, S. Shao, C. Zhang, F.-Y. Liu, Y. Wan, M. Yi, Inhibiting medial septal cholinergic neurons with DREADD alleviated anxiety-like behaviors in mice. *Neurosci. Lett.* **638**, 139–144 (2017).
34. G. Nyíri, E. Szabadits, C. Cserép, K. Mackie, R. Shigemoto, T. F. Freund, GABAB and CB1 cannabinoid receptor expression identifies two types of septal cholinergic neurons. *Eur. J. Neurosci.* **21**, 3034–3042 (2005).
35. H. K. Kia, M. J. Brisorgueil, G. Daval, X. Langlois, M. Hamon, D. Vergé, Serotonin1A receptors are expressed by a subpopulation of cholinergic neurons in the rat medial septum and diagonal band of Broca—A double immunocytochemical study. *Neuroscience* **74**, 143–154 (1996).
36. Z. Arvanitakis, R. C. Shah, D. A. Bennett, Diagnosis and management of dementia: Review. *JAMA* **322**, 1589–1599 (2019).
37. S. C. Risch, R. M. Cohen, D. S. Janowsky, N. H. Kalin, D. L. Murphy, Mood and behavioral effects of physostigmine on humans are accompanied by elevations in plasma beta-endorphin and cortisol. *Science* **209**, 1545–1546 (1980).
38. S. Pompeia, J. R. Gouveia, J. C. Galduroz, Acute mood effect of donepezil in young, healthy volunteers. *Hum. Psychopharmacol.* **28**, 263–269 (2013).
39. E. Wirkowski, I. Prohovnik, W. L. Young, Observations on the physostigmine syndrome in patients with Alzheimer's disease. *J. Neuropsychiatry Clin. Neurosci.* **3**, 73–75 (1991).
40. B. Kennedy, D. S. Janowsky, S. C. Risch, M. G. Ziegler, Central cholinergic stimulation causes adrenal epinephrine release. *J. Clin. Invest.* **74**, 972–975 (1984).
41. I. H. Richard, A. W. Justus, N. H. Greig, F. Marshall, R. Kurlan, Worsening of motor function and mood in a patient with Parkinson's disease after pharmacologic challenge with oral rivastigmine. *Clin. Neuropharmacol.* **25**, 296–299 (2002).
42. A. C. Giacomini, B. W. Bueno, L. Marcon, N. Scolari, R. Genario, K. A. Demin, T. O. Kolesnikova, A. V. Kalueff, M. S. de Abreu, An acetylcholinesterase inhibitor, donepezil, increases anxiety and cortisol levels in adult zebrafish. *J. Psychopharmacol.* **34**, 1449–1456 (2020).
43. G. Audira, N. T. Ngoc Anh, B. T. Ngoc Hieu, N. Malhotra, P. Siregar, O. Villalobos, O. B. Villaflores, T.-R. Ger, J.-C. Huang, K. H.-C. Chen, C.-D. Hsiao, Evaluation of the adverse effects of chronic exposure to donepezil (an acetylcholinesterase inhibitor) in adult zebrafish by behavioral and biochemical assessments. *Biomolecules* **10**, 1340 (2020).
44. B. Hangya, S. P. Ranade, M. Lorenc, A. Kepecs, Central cholinergic neurons are rapidly recruited by reinforcement feedback. *Cell* **162**, 1155–1168 (2015).
45. T. C. Harrison, L. Pinto, J. R. Brock, Y. Dan, Calcium imaging of basal forebrain activity during innate and learned behaviors. *Front. Neural Circuits* **10**, 36 (2016).
46. T. Laszlovszky, D. Schlingloff, P. Hegedüs, T. F. Freund, A. Gulyás, A. Kepecs, B. Hangya, Distinct synchronization, cortical coupling and behavioral function of two basal forebrain cholinergic neuron types. *Nat. Neurosci.* **23**, 992–1003 (2020).
47. X. Li, B. Yu, Q. Sun, Y. Zhang, M. Ren, X. Zhang, A. Li, J. Yuan, L. Madisen, Q. Luo, H. Zeng, H. Gong, Z. Qiu, Generation of a whole-brain atlas for the cholinergic system and mesoscopic projectome analysis of basal forebrain cholinergic neurons. *Proc. Natl. Acad. Sci. U.S.A.* **115**, 415–420 (2018).
48. X. Li, H. Yu, B. Zhang, L. Li, W. Chen, Q. Yu, X. Huang, X. Ke, Y. Wang, W. Jing, H. Du, H. Li, T. Zhang, L. Liu, L.-Q. Zhu, Y. Lu, Molecularly defined and functionally distinct cholinergic subnetworks. *Neuron* **110**, 3774–3788.e7 (2022).
49. X. Liu, M. J. Betzenhauser, S. Reiken, A. C. Meli, W. Xie, B.-X. Chen, O. Arancio, A. R. Marks, Role of leaky neuronal ryanodine receptors in stress-induced cognitive dysfunction. *Cell* **150**, 1055–1067 (2012).
50. S. Campeau, I. Liberzon, D. Morilak, K. Ressler, Stress modulation of cognitive and affective processes. *Stress* **14**, 503–519 (2011).
51. Z. Yao, C. T. J. van Velthoven, T. N. Nguyen, J. Goldy, A. E. Sedeno-Cortes, F. Baftizadeh, D. Bertagnolli, T. Casper, M. Chiang, K. Crichton, S.-L. Ding, O. Fong, E. Garren, A. Glandon, N. W. Gouwens, J. Gray, L. T. Graybuck, M. J. Hawrylycz, D. Hirschstein, M. Kroll, K. Lathia, C. Lee, B. Levi, D. M. Millen, S. Mok, T. Pham, Q. Ren, C. Rimorin, N. Shapovalova, J. Sulc, S. M. Sunkin, M. Tieu, A. Torkelson, H. Tung, K. Ward, N. Dee, K. A. Smith, B. Tasic, H. Zeng, A taxonomy of transcriptomic cell types across the isocortex and hippocampal formation. *Cell* **184**, 3222–3241.e26 (2021).
52. A. E. Cole, R. A. Nicoll, Characterization of a slow cholinergic post-synaptic potential recorded in vitro from rat hippocampal pyramidal cells. *J. Physiol.* **352**, 173–188 (1984).
53. E. Giacobini, A. C. Cuello, A. Fisher, Reimagining cholinergic therapy for Alzheimer's disease. *Brain* **145**, 2250–2275 (2022).
54. E. Joe, J. M. Ringman, Cognitive symptoms of Alzheimer's disease: Clinical management and prevention. *BMJ* **367**, l6217 (2019).
55. S. C. Risch, R. M. Cohen, D. S. Janowsky, N. H. Kalin, D. L. Murphy, Mood and behavioral effects of physostigmine on humans are accompanied by elevations in plasma β-endorphin and cortisol. *Science* **209**, 1545–1546 (1980).
56. D. Wu, D. Gao, H. Yu, G. Pi, R. Xiong, H. Lei, X. Wang, E. Liu, J. Ye, H. Yu, Y. Gao, T. He, T. Jiang, F. Sun, J. Su, G. Song, W. Peng, Y. Yang, J.-Z. Wang, Medial septum tau accumulation induces spatial memory deficit via disrupting medial septum-hippocampus cholinergic pathway. *Clin. Transl. Med.* **11**, e428 (2021).
57. G. Karvat, T. Kimchi, Acetylcholine elevation relieves cognitive rigidity and social deficiency in a mouse model of autism. *Neuropsychopharmacology* **39**, 831–840 (2014).
58. M. J. Millan, Y. Agid, M. Brüne, E. T. Bullmore, C. S. Carter, N. S. Clayton, R. Connor, S. Davis, B. Deakin, R. J. De Rubeis, B. Dubois, M. A. Geyer, G. M. Goodwin, P. Gorwood, T. M. Jay, M. Joëls, I. M. Mansuy, A. Meyer-Lindenberg, D. Murphy, E. Rolls, B. Saletu, M. Spedding, J. Sweeney, M. Whittington, L. J. Young, Cognitive dysfunction in psychiatric disorders: Characteristics, causes and the quest for improved therapy. *Nat. Rev. Drug Discov.* **11**, 141–168 (2012).
59. G. P. Mark, P. V. Rada, T. J. Shors, Inescapable stress enhances extracellular acetylcholine in the rat hippocampus and prefrontal cortex but not the nucleus accumbens or amygdala. *Neuroscience* **74**, 767–774 (1996).
60. Y. Dong, J. Mao, D. Shangguan, R. Zhao, G. Liu, Acetylcholine release in the hippocampus during the operant conditioned reflex and the footshock stimulus in rats. *Neurosci. Lett.* **369**, 121–125 (2004).
61. Y. S. Mineur, T. N. Mose, L. Vanopdenbosch, I. M. Etherington, C. Ogbejesi, A. Islam, C. M. Pineda, R. B. Crouse, W. Zhou, D. C. Thompson, M. P. Bentham, M. R. Picciotto, Hippocampal acetylcholine modulates stress-related behaviors independent of specific cholinergic inputs. *Mol. Psychiatry* **27**, 1829–1838 (2022).
62. M. Lovett-Barron, P. Kaifosh, M. A. Kheirbek, N. Danielson, J. D. Zaremba, T. R. Reardon, G. F. Turi, R. Hen, B. V. Zemelman, A. Losonczy, Dendritic inhibition in the hippocampus supports fear learning. *Science* **343**, 857–863 (2014).
63. G.-W. Zhang, W.-J. Sun, B. Zingg, L. Shen, J. He, Y. Xiong, H. W. Tao, L. I. Zhang, A non-canonical reticular-limbic central auditory pathway via medial septum contributes to fear conditioning. *Neuron* **97**, 406–417.e4 (2018).
64. B. Robert, E. Y. Kimchi, Y. Watanabe, T. Chakoma, M. Jing, Y. Li, D. B. Polley, A functional topography within the cholinergic basal forebrain for encoding sensory cues and behavioral reinforcement outcomes. *eLife* **10**, e69514 (2021).
65. L. Shen, G.-W. Zhang, C. Tao, M. B. Seo, N. K. Zhang, J. J. Huang, L. I. Zhang, H. W. Tao, A bottom-up reward pathway mediated by somatostatin neurons in the medial septum complex underlying appetitive learning. *Nat. Commun.* **13**, 1194 (2022).
66. J. C. Lemos, J. H. Shin, V. A. Alvarez, Striatal cholinergic interneurons are a novel target of corticotropin releasing factor. *J. Neurosci.* **39**, 5647–5661 (2019).
67. G. G. Calhoon, K. M. Tye, Resolving the neural circuits of anxiety. *Nat. Neurosci.* **18**, 1394–1404 (2015).
68. P. H. Janak, K. M. Tye, From circuits to behaviour in the amygdala. *Nature* **517**, 284–292 (2015).
69. Y. Sun, S. Jin, X. Lin, L. Chen, X. Qiao, L. Jiang, P. Zhou, K. G. Johnston, P. Golshani, Q. Nie, T. C. Holmes, D. A. Nitz, X. Xu, CA1-projecting subiculum neurons facilitate object-place learning. *Nat. Neurosci.* **22**, 1857–1870 (2019).
70. S. Poulter, S. A. Lee, J. Dachtler, T. J. Wills, C. Lever, Vector trace cells in the subiculum of the hippocampal formation. *Nat. Neurosci.* **24**, 266–275 (2021).
71. J. Y. Lee, H. Jun, S. Soma, T. Nakazono, K. Shiraiwa, A. Dasgupta, T. Nakagawa, J. L. Xie, J. Chavez, R. Romo, S. Yungblut, M. Hagihara, K. Murata, K. M. Igarashi, Dopamine facilitates associative memory encoding in the entorhinal cortex. *Nature* **598**, 321–326 (2021).
72. K. M. Igarashi, L. Lu, L. L. Colgin, M. B. Moser, E. I. Moser, Coordination of entorhinal-hippocampal ensemble activity during associative learning. *Nature* **510**, 143–147 (2014).
73. Y. Chen, Y. C. Lin, T. W. Kuo, Z. A. Knight, Sensory detection of food rapidly modulates arcuate feeding circuits. *Cell* **160**, 829–841 (2015).
74. I. Aklan, N. S. Atasoy, Y. Yavuz, T. Ates, I. Coban, F. Koksalar, G. Filiz, I. C. Topcu, M. Oncul, P. Dilsiz, U. Cebecioglu, M. I. Alp, B. Yilmaz, D. R. Davis, K. Hajdukiewicz, K. Saito, W. Konopka, H. Cui, D. Atasoy, NTS catecholamine neurons mediate hypoglycemic hunger via medial hypothalamic feeding pathways. *Cell Metab.* **31**, 313–326.e5 (2020).
75. Y. Yuan, W. Wu, M. Chen, F. Cai, C. Fan, W. Shen, W. Sun, J. Hu, Reward inhibits paraventricular crh neurons to relieve stress. *Curr. Biol.* **29**, 1243–1251.e4 (2019).
76. I. Lazaridis, O. Tzortzi, M. Weglage, A. Märtin, Y. Xuan, M. Parent, Y. Johansson, J. Fuzik, D. Fürth, L. E. Fenno, C. Ramakrishnan, G. Silberberg, K. Deisseroth, M. Carlén, K. Meletis, A hypothalamus-habenula circuit controls aversion. *Mol. Psychiatry* **24**, 1351–1368 (2019).
77. P. Bonnavion, A. C. Jackson, M. E. Carter, L. de Lecea, Antagonistic interplay between hypocretin and leptin in the lateral hypothalamus regulates stress responses. *Nat. Commun.* **6**, 6266 (2015).
78. N. McNaughton, B. Kocsis, M. Hajos, Elicited hippocampal theta rhythm: A screen for anxiolytic and procognitive drugs through changes in hippocampal function? *Behav. Pharmacol.* **18**, 329–346 (2007).
79. C. E. Wells, D. P. Amos, A. Jeewajee, V. Douchamps, J. Rodgers, J. O'Keefe, N. Burgess, C. Lever, Novelty and anxiolytic drugs dissociate two components of hippocampal theta in behaving rats. *J. Neurosci.* **33**, 8650–8667 (2013).
80. N. Padilla-Coreano, S. Canetta, R. M. Mikofsky, E. Alway, J. Passecker, M. V. Myroshnychenko, A. L. Garcia-Garcia, R. Warren, E. Teboul, D. R. Blackman, M. P. Morton, S. Hupalo, K. M. Tye, C. Kellendonk, D. A. Kupferschmidt, J. A. Gordon, Hippocampal-prefrontal theta transmission regulates avoidance behavior. *Neuron* **104**, 601–610.e4 (2019).

81. N. McNaughton, J. Richardson, C. Gore, Reticular elicitation of hippocampal slow waves: Common effects of some anxiolytic drugs. *Neuroscience* **19**, 899–903 (1986).
82. C. K. Monaghan, G. W. Chapman IV, M. E. Hasselmo, Systemic administration of two different anxiolytic drugs decreases local field potential theta frequency in the medial entorhinal cortex without affecting grid cell firing fields. *Neuroscience* **364**, 60–70 (2017).
83. M. E. Hasselmo, The role of acetylcholine in learning and memory. *Curr. Opin. Neurobiol.* **16**, 710–715 (2006).
84. M. E. Hasselmo, Neuromodulation: Acetylcholine and memory consolidation. *Trends Cogn. Sci.* **3**, 351–359 (1999).
85. H. A. Hartmann, L. V. Colom, M. L. Sutherland, J. L. Noebels, Selective localization of cardiac SCN5A sodium channels in limbic regions of rat brain. *Nat. Neurosci.* **2**, 593–595 (1999).
86. A. C. Bender, B. W. Luikart, P. P. Lenck-Santini, Cognitive deficits associated with Nav1.1 alterations: Involvement of neuronal firing dynamics and oscillations. *PLOS ONE* **11**, e0151538 (2016).
87. V. Satta, C. Alonso, P. Díez, S. Martín-Suárez, M. Rubio, J. M. Encinas, J. Fernández-Ruiz, O. Sagredo, Neuropathological characterization of a dravet syndrome knock-in mouse model useful for investigating cannabinoid treatments. *Front. Mol. Neurosci.* **13**, 602801 (2021).
88. Y. Niibori, S. J. Lee, B. A. Minassian, D. R. Hampson, Sexually divergent mortality and partial phenotypic rescue after gene therapy in a mouse model of dravet syndrome. *Hum. Gene Ther.* **31**, 339–351 (2020).
89. A. Bhakta, K. Gavini, E. Yang, L. Lyman-Henley, K. Parameshwaran, Chronic traumatic stress impairs memory in mice: Potential roles of acetylcholine, neuroinflammation and corticotropin releasing factor expression in the hippocampus. *Behav. Brain Res.* **335**, 32–40 (2017).
90. S. K. Prajapati, S. Krishnamurthy, Development and treatment of cognitive inflexibility in sub-chronic stress-re-stress (SRS) model of PTSD. *Pharmacol. Rep.* **73**, 464–479 (2021).
91. L. Mei, Y. Zhou, Y. Sun, H. Liu, D. Zhang, P. Liu, H. Shu, Acetylcholine muscarinic receptors in ventral hippocampus modulate stress-induced anxiety-like behaviors in mice. *Front. Mol. Neurosci.* **13**, 598811 (2020).
92. K. Mizoguchi, M. Yuzurihara, A. Ishige, H. Sasaki, T. Tabira, Effect of chronic stress on cholinergic transmission in rat hippocampus. *Brain Res.* **915**, 108–111 (2001).
93. G. M. Parfitt, R. Nguyen, J. Y. Bang, A. J. Aqrabawi, M. M. Tran, D. K. Seo, B. A. Richards, J. C. Kim, Bidirectional control of anxiety-related behaviors in mice: Role of inputs arising from the ventral hippocampus to the lateral septum and medial prefrontal cortex. *Neuropsychopharmacology* **42**, 1715–1728 (2017).
94. J. C. Jimenez, K. Su, A. R. Goldberg, V. M. Luna, J. S. Biane, G. Ordek, P. Zhou, S. K. Ong, M. A. Wright, L. Zweifel, L. Paninski, R. Hen, M. A. Kheirbek, Anxiety cells in a hippocampal-hypothalamic circuit. *Neuron* **97**, 670–683.e6 (2018).
95. M. S. Fanselow, H. W. Dong, Are the dorsal and ventral hippocampus functionally distinct structures? *Neuron* **65**, 7–19 (2010).
96. M. A. Kheirbek, L. J. Drew, N. S. Burghardt, D. O. Costantini, L. Tannenholz, S. E. Ahmari, H. Zeng, A. A. Fenton, R. Hen, Differential control of learning and anxiety along the dorsoventral axis of the dentate gyrus. *Neuron* **77**, 955–968 (2013).
97. T. Bast, I. A. Wilson, M. P. Witter, R. G. Morris, From rapid place learning to behavioral performance: A key role for the intermediate hippocampus. *PLOS Biol.* **7**, e1000089 (2009).
98. B. A. Strange, M. P. Witter, E. S. Lein, E. I. Moser, Functional organization of the hippocampal longitudinal axis. *Nat. Rev. Neurosci.* **15**, 655–669 (2014).

Acknowledgments

Funding: This work was supported by grants from the STI2030-Major Projects (2021ZD0202704), the National Natural Science Foundation of China (82090032 and 31830033), the Key-Area Research and Development Program of Guangdong Province (2018B030334001 and 2018B030340001), the Science and Technology Program of Guangzhou (202007030013), and the Guangdong Basic and Applied Basic Research Foundation (2022A1515011987). **Author contributions:** Conceptualization: T.-M.G. Methodology: J.-L.W., Z.-M.L., and Y.-H.C. Investigation: J.-L.W., Z.-M.L., H.C., N.-Y.H., and S.-Y.J. Visualization: J.-L.W., W.-J.C., Y.-H.C., and T.-M.G. Supervision: J.-L.W. and T.-M.G. Writing—original draft: J.-L.W. and T.-M.G. Writing—review and editing: J.-L.W., Y.-H.C., and T.-M.G. Data curation: J.-L.W. Formal analysis: J.-L.W., Z.-M.L., N.-Y.H., and J.-M.Y. Software: N.-Y.H. Resources: Z.-M.L., N.-Y.H., S.-Y.J., X-W.L., Y.-H.C., and T.-M.G. Validation: J.-L.W., Z.-M.L., N.-Y.H., S.-Y.J., and Y.-H.C. Funding acquisition: J.-L.W. and T.-M.G. Project administration: J.-L.W. and T.-M.G. **Competing interests:** The authors declare that they have no competing interests. **Data and materials availability:** All data needed to evaluate the conclusions in the paper are present in the paper and/or the Supplementary Materials.

Submitted 18 January 2024
Accepted 7 October 2024
Published 8 November 2024
10.1126/sciadv.ado1508